JCI The Journal of Clinical Investigation

S1PR4 ablation reduces tumor growth and improves chemotherapy via CD8+ T cell expansion

Catherine Olesch, … , Bernhard Brüne, Andreas Weigert

J Clin Invest. 2020. https://doi.org/10.1172/JCI136928.

Research In-Press Preview **Immunology** **Oncology**

Graphical abstract

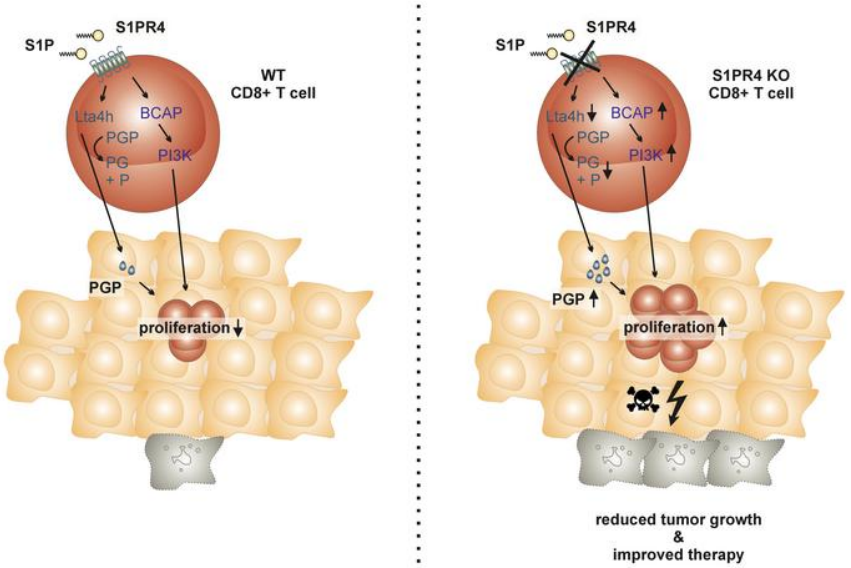

S1PR4 ablation reduces tumor growth and improves chemotherapy via CD8+ T cell expansion

Catherine Olesch[1], Evelyn Sirait-Fischer[1], Matthias Berkefeld[1], Annika F. Fink[1], Rosa M. Susen[1], Birgit Ritter[2,3], Birgitta E. Michels[2,3,4], Dieter Steinhilber[5], Florian R. Greten[2,3,4], Rajkumar Savai[3,6,7], Kazuhiko Takeda[8], Bernhard Brüne[1,3,4,9], and Andreas Weigert[1,3,4*]

[1]Institute of Biochemistry I, Faculty of Medicine, Goethe-University Frankfurt, 60590 Frankfurt, Germany

[2]Institute for Tumor Biology and Experimental Therapy, Georg-Speyer-Haus, 60590 Frankfurt, Germany

[3]Frankfurt Cancer Institute (FCI), Goethe-University Frankfurt, 60596 Frankfurt, Germany

[4]German Cancer Consortium (DKTK), Partner Site Frankfurt, Germany

[5]Institute of Pharmaceutical Chemistry, Goethe University Frankfurt, 60438 Frankfurt, Germany

[6]Max Planck Institute for Heart and Lung Research, Member of the German Center for Lung Research (DZL), Member of the Cardio-Pulmonary Institute (CPI), Bad Nauheim, 61231, Germany

[7]Institute for Lung Health (ILH), Justus Liebig University, 35392, Giessen, Germany

[8]Research Center of Oncology, ONO Pharmaceutical co., ltd., Osaka, Japan

[9]Branch for Translational Medicine and Pharmacology TMP of the Fraunhofer Institute for Molecular Biology and Applied Ecology IME, 60590 Frankfurt, Germany

Short title: S1PR4 restricts CD8+ T cell expansion in cancer

Keywords: cancer, inflammation, sphingolipids, cytotoxic T cells

*Correspondence to:

Andreas Weigert

Goethe-University Frankfurt

Faculty of Medicine

Institute of Biochemistry I - Pathobiochemistry

Theodor-Stern-Kai 7, 60590 Frankfurt, Germany

Phone: +49-69-6301-4593

Fax: +49-69-6301-4203

Email: weigert@biochem.uni-frankfurt.de

Conflict of interest disclosure: The authors declare no potential conflicts of interest.

Abstract

Tumor immunosuppression is a limiting factor for successful cancer therapy. The lipid Sphingosine-1-phosphate (S1P), which signals through five distinct G-protein-coupled receptors (S1PR1-5), emerged as an important regulator of carcinogenesis. However, the utility of targeting S1P in tumors is hindered by its impact on immune cell trafficking. Here we report that ablation of the immune cell-specific receptor S1PR4, which plays a minor role in immune cell trafficking, delayed tumor development and improved therapy success in murine models of mammary and colitis-associated colorectal cancer due to an increased CD8+ T cell abundance. Transcriptome analysis revealed that S1PR4 affected proliferation and survival of CD8+ T cells in a cell-intrinsic manner via the expression of *Pik3ap1* and *Lta4h*. Accordingly, PIK3AP1 expression was connected to increased CD8+ T cell proliferation and clinical parameters in human breast and colon cancer. Our data indicate a so far unappreciated tumor-promoting role of S1P by restricting CD8+ T cell expansion via S1PR4.

Introduction

The impact of the immune system on tumor progression is multifaceted. While inflammation may promote cancer progression, data obtained from animal models and clinical studies demonstrate that the immune system is inherently capable of tumor recognition and rejection. One of the key effector cells of anti-tumor immunity are cytotoxic CD8+ T cells. The number of CD8+ T cells in human breast and colon tumors is positively correlated to cancer-free survival (1, 2). More specifically, the abundance of distinct CD8+ T cell subtypes, particularly effector and memory CD8+ T cells versus exhausted CD8+ T cells, is predictive of either a pro- or an anti-tumor response. Effector CD8+ T cells develop from naïve T cells upon T cell priming and are highly toxic to tumor cells through secretion of IFNγ, TNFα, perforin and granzyme B. They are usually short-lived cells that undergo apoptosis upon elimination of the antigen. However, a small proportion of antigen-specific tissue-resident memory (Trm) CD8+ T cells persist, which can rapidly differentiate into effector T cells upon a repeated antigen challenge. During cancer progression the proportion of exhausted CD8+ T cells increases. These cells are characterized by reduced cytotoxic activity, proliferation and the up-regulation of inhibitory immune checkpoint receptors such as programmed cell death protein 1 (PD-1). Thus, targeting mechanisms that restrict anti-tumor CD8+ T cell expansion and/or activity is of immense benefit in cancer therapy. Molecules blocking inhibitory immune checkpoints have shown clinical efficacy, however, only a subset of patients benefit from such approaches (3). Therefore, the discovery of new targets is warranted to restore anti-tumor immunity or to prime for immune checkpoint blockade.

Sphingolipid sphingosine-1-phosphate (S1P) is present in low concentrations in most tissues under homeostatic conditions, with the exception of blood and lymph. In the circulation, S1P acts as a major chemoattractant for lymphocytes entering the

circulation from peripheral and lymphoid tissues (4). In tumors, the levels of S1P are elevated due to the deregulation of S1P-synthesizing and degrading enzymes or as a consequence of tumor cell death (4-6). Once produced, S1P supports carcinogenesis by promoting tumor growth, angiogenesis and metastasis (7). S1P exerts its functions by either binding to intracellular targets or to its five known G-protein-coupled receptors (S1PR1–5), which differ in terms of cellular expression profile and function (8). Targeting the S1P system systemically or targeting migratory S1P receptors such as S1PR1 may affect lymphocyte trafficking into tumors and consequently prevent anti-tumor immunity. Although, S1PR4 is highly expressed in lymphocytes, it does not affect lymphocyte trafficking (9). Rather, S1PR4 is linked to the regulation of myeloid cell activation, which in turn may affect lymphocyte responses (10, 11). Currently, the role of S1PR4 in tumor immunity is elusive. Therefore, we investigated whether ablation of S1PR4 may affect tumor growth without inducing immune paralysis.

Results

S1PR4 promotes mammary tumor progression and limits CD8+ T cell abundance

We crossed mice harboring a global S1PR4 knockout (KO) into the polyoma middle T (PyMT) background to test whether S1PR4 signaling affects tumor-associated inflammation (12). In this background, the PyMT oncoprotein is expressed in the mammary epithelium initiating mammary tumor formation starting from 6–8 weeks postnatal and the occurrence of pulmonary metastases after 16–20 weeks (13). At the ethical endpoint (i.e., when the first mammary tumor reached a diameter of ~ 1.5 cm), WT or S1PR4 KO PyMT animals did not show difference in tumor burden (Figure 1A). However, tumors of S1PR4 KO PyMT mice required significantly longer time to reach the endpoint, indicating a S1PR4-dependent delay in tumor growth (Figure 1B). Moreover, histochemical analyses of lungs revealed a significantly decreased number of metastases in S1PR4 KO PyMT mice despite similar tumor burden, suggesting an additional impact on metastasis (Figure 1C, D). We generated comprehensive FACS profiles of WT and S1PR4 KO PyMT tumors to investigate the immune contexture upon S1PR4 KO (Suppl. Figure 1 exemplary for WT PyMT tumor). We found no significant change in the frequency of CD45+ cells within PyMT tumors *per se*, which was confirmed by immunohistochemistry (Suppl. Figure 2B, G-H). No individual immune cell subset was altered (Figure 2A-C), with the exception of a markedly increased abundance of cytotoxic CD8+ T cells in S1PR4 KO PyMT tumors (Figure 2A, D), which was confirmed by immunohistochemistry (Figure 2E, F). Further characterization of tumor-infiltrated CD8+ T cell subtypes thereby indicated that mainly exhausted CD8+ PD-1+ and effector CD8+ T cells were increased when S1PR4 was absent (Figure 2G). S1PR4-dependent changes in the CD8+ T cell infiltrate were restricted to the tumor site since CD8+ T cell counts were unchanged in the spleen, mesenteric lymph nodes (LNs), tumor-draining axillary LNs and lungs of S1PR4 KO PyMT mice

compared with their WT counterparts (Suppl. Figure 2A, C-F). S1PR4 is known to affect T cell function indirectly through activation of myeloid cells (9). Thus, we determined if number and/or suppressive activity of myeloid-derived suppressor cells (MDSCs) were reduced upon S1PR4 KO, explaining enhanced CD8+ T cell infiltrates in KO PyMT tumors. We performed intracellular staining of the T cell-suppressive MDSC marker arginase 1 (Arg1) and analyzed the number of infiltrating granulocytic CD11b+ Ly6G high Ly6C low MDSCs (gMDSC) and monocytic CD11b+ Ly6G low Ly6C high MDSCs (mMDSCs) expressing this marker in tumors of WT and S1PR4 KO PyMT mice. However, neither the number of Arg1+ gMDSCs nor Arg1+ mMDSCs was changed in S1PR4 KO PyMT tumors compared to their WT counterpart (Figure 2H). Next, we performed a MDSC suppression assay, for which in vitro differentiated WT and S1PR4 KO MDSCs were co-cultured in different ratios with cell proliferation dye eFluor® 670-prelabeled splenocytes of WT mice. Analysis of T cell proliferation revealed no difference in the suppressive activity of S1PR4 KO MDSCs compared to the WT control group (Figure 2I). Next, chemokine protein levels of WT and S1PR4 KO tumors were determined to assess whether S1PR4-dependent differences in tumor-specific CD8+ T cell infiltrates resulted from a different migrational behaviour of CD8+ T cells in tumors. Only protein level of C-C motif chemokine ligand 11 (CCL11) was significantly reduced in S1PR4 KO PyMT tumors, while other chemokines remained unchanged (Figure 2J). Moreover, Boyden chamber migration assays did not reveal major differences in the migration of CD45+ splenocytes (e.g., total T cells, CD8+ T cells, CD4+ T cells and regulatory T cells (Tregs)) towards S1PR4 WT versus KO tumor fluids (Figure 2K). These data indicate that the alterations in the abundance of CD8+ T cells in S1PR4 KO tumors were likely independent of MDSCs and CD8+ T cell recruitment.

S1PR4 favors colitis-associated cancer and restricts epithelial CD8+ T cell expansion

Breast cancer is known for its weak immunogenicity and immunosuppressive tumor microenvironment (14). We asked if S1PR4 ablation in a strictly inflammation-driven tumor mouse model would cause a stronger impact on tumor growth compared with the PyMT model. Therefore, WT and S1PR4 KO mice were subjected to the azoxymethane (AOM)/dextran sulfate sodium (DSS) model of colitis-associated cancer (CAC) and colon tissues were analyzed at time points reflecting the different phases of CAC development in this model (i.e., day 8, inflammation; day 15, regeneration; day 84, colon tumors) (Figure 3A). S1PR4 KO did not reduce initial inflammation in the AOM/DSS model based on the absence of changes in relative weight loss, the lamina propria (LP) immune infiltrate at day 8, colon histology and colon weight to length ratio (Figure 3B-F). The colon weight to length ratio was different at the basal level in untreated mice, which was lost during colon inflammation. However, it was significantly reduced at day 84 in S1PR4 KO mice following the full development of colon tumors (Figure 3F). This observation was accompanied by almost no tumor development in KO mice (Figure 4A, B), although ablation of S1PR4 did not affect initial inflammation. FACS analysis (Suppl. Figure 3A) did not indicate major changes in the immune cell profile between WT and S1PR4 KO LP at distinct time-points (Figure 3C, D). Analysis of the epithelial immune cell fraction revealed that total intraepithelial lymphocytes (IEL), CD8+ IEL and CD8+ IEL with a Trm phenotype (CD103+) were unchanged at days 0 and 8 between WT and S1PR4 KO mice (Suppl. Figure 3B). However, these subsets started to increase at day 15 and remained elevated at day 84 in the S1PR4 KO epithelial fraction (Figure 4C-E). Further characterization of other CD8+ IEL subsets in colons of day 84 revealed significantly enhanced effector CD8+ IEL similar to the PyMT model, whereas the number of exhausted CD8+ PD-1+ IEL was unchanged in this model when S1PR4 was absent (Suppl. Figure 3C). These findings indicated that late expansion and survival of protective effector T cells rather than

altered initial inflammation may underlie reduced tumor development in AOM/DSS-treated S1PR4 KO mice. Of note, the number of Arg1+ gMDSCs and mMDSCs were also unchanged in LP of S1PR4 KO mice at day 84 compared to the WT control (Suppl. Figure 3D). In conclusion, in both the PyMT and AOM/DSS models, ablation of S1PR4 delayed tumor growth and was accompanied by an increase of intra-tumoral effector CD8+ T cells.

S1PR4 depletion improves response to chemotherapy through CD8+ T cells

Since ablation of S1PR4 in both, the PyMT and AOM/DSS model showed a simultaneous delay in tumor growth and enhanced abundance of CD8+ T cells, we next asked for a tumor model suitable to analyze if both phenomena were causatively linked. To this end, we used a neutralizing approach in a therapeutic PyMT chemotherapy model rather than in the standard PyMT or the AOM/DSS model for several reasons. Firstly, in the latter models the time-point at which CD8+ T cells may start interfering with tumor growth is unclear. Secondly, the chemotherapy approach with doxorubicin (DXR) induces tumor cell death, resulting in amongst others enhanced secretion of S1P (6), thus boosting the impact of S1PR4 ablation. We deemed this boosting effect of chemotherapy necessary since tumor growth reduction in the S1PR4 KO PyMT mice was rather minor. Thus, we aimed to analyze if enhancing immunogenicity by treating PyMT mice with DXR resulted in a more pronounced tumor growth reduction comparable to the AOM/DSS model. WT and S1PR4 KO PyMT mice were treated with DXR once-weekly for 5 weeks from the time when the first tumor reached a diameter of ~ 1.3 cm (Figure 5A). During treatment of WT PyMT mice with DXR, the tumor size initially decreased before increasing again after the 3rd to 4th administration of DXR, indicating tumor relapse (Figure 5B). S1PR4 KO PyMT tumors responded to DXR treatment without tumor relapse. Importantly, CD8+ T cells

remained strongly elevated in DXR-treated S1PR4 KO PyMT tumors (Figure 5C, D). Further characterization of tumor-infiltrated CD8+ T cell subsets revealed that memory CD8+ Trm were significantly enhanced and exhausted CD8+ PD-1+, with a trend towards increased effector CD8+ T cells in DXR-treated S1PR4 KO PyMT tumors (Figure 5E). This elevation of total CD8+ T cells appeared to be crucial, as the improved response of S1PR4 KO PyMT mice to chemotherapy was effectively abolished following the depletion of CD8+ T cells using a CD8 neutralizing antibody compared to an isotype control (Figure 5F). The CD8 antibody depleted CD8 from the cell surface as indicated by a reduction of about 97% in the number of CD8+ T cells compared with the IgG control (Suppl. Figure 4A). However, this effect was accompanied by an increase in double negative (DN) T cells, thus excluding an impact of T cell death on tumor growth (Figure 5G). The increased presence of DN T cells suggests a mechanism how the anti-CD8 antibody interfered with CD8+ T cell function, namely by reducing CD8 surface expression and thereby preventing MHCI engagement and target cell killing. Along this line, we excluded non-specific Fc receptor activation of macrophages by the IgG control and CD8 antibodies, since stimulation of bone-marrow derived WT macrophages with these antibodies neither changed morphology, CD80/86 expression nor anti- and pro-inflammatory cytokine secretion (Suppl. Figure 4B-H).

Since the characterization of intra-tumoral CD8+ T cells revealed enhanced abundance of exhausted PD-1+ CD8+ T cells in S1PR4 KO tumors (Figure 2G), but not in the AOM/DSS model, we asked if S1PR4 KO might sensitize PyMT tumors to immune checkpoint blockade and thus also provide a therapy advantage. Once the first tumor reached a diameter of 0.6 cm, WT and S1PR4 KO PyMT mice were injected with either anti-PD-1 antibody or an isotype control (IgG1) at days 0, 6, 12, and 18 (Figure 6A). FACS analysis confirmed the effective depletion of PD-1 in CD8+ T cells

and the S1PR4-dependent increase of CD8+ T cells in tumors of IgG control, as well as in mice treated with anti-PD-1. Nonetheless, there was no additional increase in CD8+ T cells following the neutralization of PD-1 in S1PR4 KO mice (Figure 6B). As we also previously reported (15), anti-PD-1 treatment in WT mice showed only poor therapeutic efficacy (Figure 6C). However, while ablation of S1PR4 decreased tumor progression, treatment with anti-PD-1 showed only a minor additional effect (Figure 6D). Type I interferons (IFNα, IFNβ) can act as chronic regulators of the PD-1/PD-L1 signaling axis, and we already previously linked S1PR4 ablation to enhanced IFNα production (10, 16, 17). Thus, we asked if S1PR4 ablation in PyMT mice lead to enhanced IFN signaling, which would potentially be linked to increased abundance of intra-tumoral CD8+ PD-1+ T cells. Indeed, both *Ifna* and *Ifnb* expression were increased in S1PR4 KO tumors, with *Ifna* being significantly enhanced at mRNA level (Figure 6E). To test if IFN signaling was responsible for enhanced abundance of CD8+ PD-1+ T cells in S1PR4 KO PyMT tumors, we crossed WT and S1PR4 KO PyMT mice with interferon-A/B receptor 1 (IFNAR1) WT and KO mice. When the first PyMT tumor reached a diameter of ~ 1.5 cm the immune contexture of tumors was analyzed by FACS. Whereas CD8+ PD-1+ T cells were increased in tumors of IFNAR1 WT S1PR4 KO (IWSK) PyMT mice compared to the WT control group (IWSW), this effect was abolished in IFNAR1 KO S1PR4 KO (IKSK) PyMT mice (Figure 6F). These data demonstrated that enhanced abundance of CD8+ PD-1+ T cells in S1PR4 KO PyMT tumors resulted from increased signaling through type I interferons when S1PR4 was absent. However, whereas ablation of S1PR4 sensitized cells to chemotherapy, immune checkpoint blockade with PD-1-neutralizing antibody only mildly improved therapy efficacy. Thus, these data suggest that S1PR4 restricts the expansion of functional anti-tumor CD8+ T cells, thereby limiting chemotherapy success.

S1PR4 restricts CD8+ T cell expansion in a cell-intrinsic manner

We observed that the increase in CD8+ T cell numbers upon S1PR4 ablation was tumor-specific and independent of cell recruitment. Thus, we explored other mechanisms of CD8+ T cell expansion in tumors which may be affected by S1PR4. To this end, we compared whole transcriptome signatures of FACS-sorted CD8+ T cells from PyMT tumors of WT and S1PR4 KO mice (Figure 7A). Gene set enrichment analysis (GSEA) identified enriched specific pathways in S1PR4 KO CD8+ T cells related to proliferation, survival or activation while there was no specific enrichment of immune signatures or cell recruitment related to CD8+ T cells (Figure 7B, C; Suppl. Table 1). However, WT CD8+ T cells showed enrichment of genes characterizing naïve T cells. This result indicated that, in mammary carcinoma S1PR4 KO favored a CD8+ T cell memory response (Suppl. Table 1). This notion was supported by the DXR model, where an enrichment of CD8+ T cells showing a Trm phenotype was observed after ablation of S1PR4 (Figure 5E). Additionally, this enrichment corresponded to the increase in CD8+ Trm in the epithelial fraction of S1PR4 KO colons in the AOM/DSS model at day 84 (Figure 4E). Thus, ablation of S1PR4 appeared to alter CD8+ T cell proliferation, survival, and memory formation in mammary tumors *in situ*. S1PR4 was mainly expressed by T cells and neutrophils, at low levels by macrophages and endothelial cells and was absent in tumor cells (Suppl. Figure 5A). Importantly, besides S1PR1, S1PR4 was the predominant S1P receptor expressed by murine CD8+ T cells (Suppl. Figure 5B). Due to the prominent expression by CD8+ T cells, we hypothesized that the impact of S1PR4 on CD8+ T cell expansion may occur in a cell-intrinsic manner. To test this hypothesis, we performed T cell proliferation assays using splenic CD8+ T cells isolated from WT and S1PR4 KO mice, pre-activated with CD3/28 T cell activator beads and maintained in culture for up to two weeks to allow memory formation. Flow cytometry was used to determine the absolute cell number over time.

A significant increase in CD8+ T cells upon ablation of S1PR4 was observed at day 2 after activation. This was followed by a lower plateau phase at day 8, which, however, resulted in a higher number of surviving CD8+ S1PR4 KO T cells thereafter (Figure 7D). Expression of the proliferation marker *Ki67* combined with Annexin V/7-AAD FACS analysis at day 2 suggested that both enhanced proliferation and survival were associated with increased CD8+ T cell numbers (Figure 7E, F). The higher S1PR4 KO CD8+ T cell count which we observed from day 10 onwards suggested enhanced overall survival, which again was confirmed by AnnexinV/7-AAD staining (Figure 7F). Following the notion that T cells which survive repeated antigen stimulation develop into memory cells, we observed significantly more CD8+ T cells harboring a Trm phenotype after ablation of S1PR4 (Figure 7G). This indicates that S1PR4 expressed on CD8+ T cells restricts activation-induced proliferation, survival and the abundance of CD8+ Trm cells following TCR activation in a cell-intrinsic manner.

To identify molecular mechanisms of reduced CD8+ T cell expansion downstream of S1PR4, we compared whole transcriptome signatures of colon tissue of AOM/DSS-treated mice (day 84) with those of FACS-sorted CD8+ T cells from PyMT tumors, (S1PR4 KO compared to WT mice). 491 upregulated and 350 downregulated genes were identified in AOM/DSS-treated S1PR4 KO colons (red segments, Figure 8A). 87 upregulated and 516 downregulated genes were observed in FACS-sorted PyMT CD8+ T cells (blue segments, Figure 8A). Of note, 24 upregulated and 23 downregulated genes were shared between both tumor models (yellow segments, Figure 8A). Importantly, targets such as DNA topoisomerase 2 alpha (*Top2a*) and DNA polymerase epsilon/theta (*Pole*/*Polq*) were upregulated in the S1PR4 KO setting in both groups, suggesting increased proliferation. The calcium/calmodulin dependent protein kinase 2 beta (*Camk2b*) and phosphoinositide-3-kinase adaptor protein 1 (*Pik3ap1*) genes were previously linked to T cell proliferation and/or survival (18, 19).

Therefore, we selected these genes for in vitro validation in the T cell proliferation assay to understand the molecular mechanisms of increased proliferation. CAMK2B is involved in calcium signaling, whereas PIK3AP1 is a positive regulator of PI3K signaling (20, 21). Additionally, we selected the leukotriene B4-synthesizing enzyme LTA4H, based on its consistent downregulation and the findings that leukotrienes may affect CD8+ T cell function (22). Analysis of mRNA expression of the selected targets during the course of T cell proliferation revealed alterations in the expression of *Camk2b*, *Pik3ap1* and *Lta4h* expression in S1PR4 KO T cells. Thereby, *Camk2b* showed a robust upregulation, whereas *Lta4h* was downregulated at each analyzed time point (Suppl. Figure 5C, D). The expression of *Pik3ap1* appeared more relevant in untreated T cells and at later time points post-activation (Suppl. Figure 5E). Using pharmacological inhibitors of CAMK2B, PIK3AP1 and LTA4H-dependent pathways in the T cell proliferation assay showed that a low dose of the PI3K inhibitor Ly294002 reduced S1PR4 KO T cell levels to those of WT CD8+ T cells at day 2 (Figure 8B). On the other hand, the LTA4H inhibitor SC 57461A increased WT T cell numbers to a level similar to that of S1PR4 KO CD8+ T cells (Figure 8C), whereas the CaM kinase 2 inhibitor Autocamtide-2-related inhibitory peptide (AIP) did not affect the numbers of T cells at day 2 (Suppl. Figure 5F). This translated into anti-tumor efficacy of CD8+ T cells against PyMT tumor cells. 3D PyMT tumor spheroids were infiltrated with untreated, pre-treated (Ly294002 or SC 57461A) WT or S1PR4 KO CD8+ T cells, with the addition of IL-2 at days 2 and 4 following infiltration. This treatment reduced the spheroid size within two days following the second administration of IL-2 (day 6) (Figure 8D, E). The spheroid diameter was significantly reduced at day 6 after infiltration with S1PR4 KO CD8+ T cells (Figure 8F, G); however, this effect was abolished after inhibition of PI3K (Figure 8D, H). On the other hand, a significant

reduction in spheroid size was observed after pre-treatment of WT CD8+ T cells with the LTA4H inhibitor (Figure 8F, I).

For a more detailed mechanistic insight into the S1PR4-dependent function downstream of PIK3AP1, the gene was knocked down in WT and S1PR4 CD8+ T cells. Since PIK3AP1 is known to enforce PI3K signaling, enhanced *Pik3ap1* expression in S1PR4 KO CD8+ T cells should potentiate PI3K signaling, leading to enhanced phosphorylation of AKT. Thus, WT and S1PR4 KO CD8+ T cells treated with non-target control (NTC) and PIK3AP1 siRNA were stained intracellularly for phospho-AKT (pAKT) after activation. A robust PIK3AP1 knockdown was achieved with a reduction of ~50% of *Pik3ap1* expression (Suppl. Figure 5G). Protein expression of pAKT was analyzed as mean fluorescence activity (MFI) by flow cytometry. Indeed, AKT phosphorylation was significantly enhanced in S1PR4 KO CD8+ T cells after activation, but abolished when S1PR4 KO CD8+ T cells were treated with PIK3AP1 siRNA (Figure 8I). These data demonstrated that enhanced *Pik3ap1* expression potentiated pAKT/PI3K signaling, which enhanced CD8+ T cell proliferation and increased tumor control as shown by inhibiting PI3K with Ly294002.

Next we asked for a mechanism of enhanced T cell proliferation downstream of S1PR4-dependent up-regulation of *Lta4h* expression. The leukotriene LTA4 produced by 5-lipoxygenase is converted to LTB4 by LTA4H or alternatively converted to cysteinyl leukotrienes (23). We first asked if shunting towards cysteinyl leukotrienes upon decrease of *Lta4h* expression was enhanced. However, we did not detect differences in cysteinyl leukotriene (CysLT) LTC4, LTD4 and LTE4 levels in supernatants of activated CD8+ S1PR4 KO T cells compared to the WT control (Suppl. Figure 5H). Also, CysLT receptor 1 (CysLT1R) inhibition using Montelukast did not affect CD8+ T cell proliferation, and CysLT2R inhibition by HAMI3379 even further enhanced CD8+ T cell numbers of WT and S1PR4 KO mice (Suppl. Figure 5I). LTA4H

exhibits a dual catalytic activity including hydrolase activity responsible for the conversion of LTA4 to LTB4 and an aminopeptidase activity essential for the degradation of the chemotactic tripeptide Pro-Gly-Pro (PGP) (24). While we indeed found that reduced *Lta4h* expression in CD8+ S1PR4 KO T cells resulted in diminished LTA4 to LTB4 conversion (Figure 8J), addition of LTB4 increased proliferation of both WT and S1PR4 KO CD8+ T cells in the T cell proliferation assay (Suppl. Figure 5J), which was described before (25). Moreover, a role for the hydrolase activity was finally excluded when specifically LTA4 to LTB4 conversion was inhibited by 4-[4-(phenylmethyl)phenyl]-2-thiazolamine Arm1. Stimulating WT CD8+ T cells with S1PR4 agonist (Cym50308) and antagonist (Cym50358) in addition to Arm1 did not affect enhanced CD8+ T cell expansion when S1PR4 was inhibited (Suppl. Figure 5K). Of note, treatment of WT CD8+ T cells with S1PR4 antagonist Cym50358 resulted in a comparable increase of CD8+ T cells as genetic ablation of S1PR4 (Suppl. Figure 5L). Thus, we hypothesized that reduced S1PR4-dependent *Lta4h* expression diminished aminopeptidase activity of LTA4H resulting in reduced degradation of PGP. Indeed, when synthetic PGP was added to S1PR4 agonist or antagonist treated CD8+ T cells, cell numbers of both groups increased significantly and thereby abolished enhanced proliferation of S1PR4 antagonist treated CD8+ T cells (Figure 8K). Interestingly, PGP was also connected to S1PR4-dependent CD8+ T cell survival, as PGP enhanced survival of S1PR4 agonist treated CD8+ T cells to a level similar to of S1PR4 antagonist treated CD8+ T cells (Figure 8L). Unfortunately, measuring PGP levels would have required serum-free conditions, which were not compatible with the T cell proliferation assay. In conclusion, PIK3AP1/PI3K and LTA4H/PGP signaling appear as cell-intrinsic drivers of the S1PR4-dependent restriction of CD8+ T cell expansion.

S1PR4-dependent alterations in CD8+ T cells are linked to progression of human cancer

We subsequently used a human peripheral blood mononuclear cell/MCF-7 (PBMC/MCF-7) mammary tumor cell spheroid co-culture system with or without pre-treatment of human PBMCs with the S1PR4 agonist Cym 50308 or the S1PR4 antagonist Cym 50358. Use of the S1PR4 antagonist resulted in a significant increase in CD8+ T cells, whereas S1PR4 agonist did not alter the number of CD8+ T cells (Figure 9A). Based on this observation we asked if S1PR4 signaling may also be relevant for human cancer. Analysis of publicly available cancer datasets showed that the correlation of S1PR4 expression with clinical parameters was irrelevant. S1PR4 is mainly expressed on lymphocytes, therefore its expression reflects the number of tumor-infiltrated lymphocytes, which is often correlated with enhanced breast cancer patient survival. As an alternative, we generated an in silico S1P production ratio by comparing the mean mRNA expression of S1P producing (SPHK1/2) versus S1P degrading (SGP1, SGPP1/2, and PPAP2B) enzymes at mRNA level. This S1P ratio was then compared to CD8+ T cell abundance and overall survival using the METABRIC mammary carcinoma and the provisional TCGA colorectal adenocarcinoma datasets (26, 27). Apparently a high S1P ratio, which may indicate increased S1P levels, was correlated to reduced breast cancer patient survival (Figure 9B, S1P ratio Q4). Furthermore, a high S1P ratio was also correlated to reduced CD8A as well as CD103 expression within human breast tumors (Figure 9C, D). The same pattern was observed for the colorectal carcinoma dataset (Figure 9E-G). These correlation data indicated that enhanced S1P production, potentially via S1PR4 restricts the abundance of human CD8+ T cells and CD103+ Trm and correlated with reduced patient survival. We subsequently analyzed whether molecular alterations downstream of S1PR4 identified in mouse tumors and through the in vitro T cell

proliferation assay were relevant in human cancer. More specifically, we aimed to analyze if enhanced abundance of PIK3AP1+ CD8+ T cells and diminished LTA4H+ CD8+ T cell numbers correlated with reduced disease severity in cancer patients. We performed PhenOptics multispectral immunostaining in tissue microarrays (TMAs) of patients with colon adenocarcinoma and mammary carcinoma. In human tumor sections only a small number of CD8+T cells expressed LTA4H. Notably, the expression of PIK3AP1 was heterogeneous, with some tumors showing high numbers of CD8+ PIK3AP1+ T cells, which were then often proliferative (Figure 9H, Suppl. Figure 6A-C). In colon carcinoma TMA sections, the expression of PIK3AP1 indeed correlated with KI67 expression in CD8+ T cells, but not with LTA4H expression. Moreover, a high abundance of PIK3AP1+ CD8+ T cells was correlated with reduced tumor cell proliferation, nodal involvement, stage and metastasis (Figure 9I). Interestingly, there was a positive correlation of LTA4H expression with metastasis, although the importance of this pattern is limited by the low number of metastatic tumors in this tissue set. In mammary carcinoma TMA sections, the presence of CD8+ T cells showed a tendency towards positive correlation with patient survival. This tendency reached significance when CD8+ T cells were additionally positive for PIK3AP1 and was lost when positive for LTA4H (Figure 9J-L, Suppl. Figure 6C).

Discussion

S1P levels are elevated in tumors, which is associated with poor prognosis for cancer patients (28). Accordingly, the various aspects of S1P production, degradation or signalling have emerged as putative drug targets in cancer (29). However, approaches targeting S1P levels globally, such as a S1P-neutralizing antibody or a pharmacological inhibitor of SPHK2 revealed limited success in clinical studies (30, 31). A reason may be that, while SPHK-derived S1P has both intracellular and extracellular targets that promote tumor growth at the tumor cell level, its impact in the tumor stroma is more diverse. While S1PR1 signaling in tumor-associated myeloid cells and other immune cells promotes tumor growth and metastasis in a number of tumor models (32-36), S1PR2 on myeloid cells may limit these features (37). Thus, targeting S1PR1 in cancer appears promising. However, S1PR1 inhibits sprouting angiogenesis, Moreover, S1PR1 antagonists (e.g., FTY720) induce immune paralysis by trapping lymphocytes in lymphatic organs, thereby restricting their access to the tumor (38). These two features of S1PR1 blockade are not desired in tumors (39, 40). Importantly, murine CD8+ T cells preferentially expressed S1PR1 and S1PR4. Thus, S1PR4 appears as the only reasonable candidate among S1P receptors to improve their function in a tumor context. Our data thus indicate that S1PR4 might be an interesting target, particularly in combination with conventional therapy.

S1PR4 is expressed at high levels mainly by lymphocytes and neutrophils. Although S1PR4 was recently shown to play a role in CD4+ T cell transmigration in a lymphatic context (41). However, S1PR4-deficient mice do not show defects in lymphocyte composition in lymphatic organs as shown in this and another study (42). Transfer of labelled WT and S1PR4 KO T cells in WT mice revealed that rapid (within 2.5 h) recruitment of CD8+ T cells to LNs was enhanced in the absence of S1PR4, whereas this difference was lost at 24 h (43). Thus, S1PR4 plays only a minor regulatory role in

T cell migration in vivo. In our experiments (AOM/DSS and PyMT + DXR; data not shown for the latter) CD8+ T cells started to increase at the tumor site within weeks rather than hours. In the AOM/DSS model, this increase coincided with the initiation of cell transformation and thus the start of tumor development. This suggests the presence of a mechanism other than recruitment as the underlying reason for the accumulation of CD8+ T cells in tumors after ablation of S1PR4.

Rather, ablation of S1PR4 increased the T cell receptor-driven proliferation of CD8+ T cells and/or subsequent memory formation. This was a tumor-specific effect, considering that the number of CD8+ T cells was not elevated in other tissues. Moreover, GSEA analysis in tumor-infiltrating CD8+ T cells strongly supported the local proliferation in the absence of S1PR4. Enhanced T cell proliferation in vitro was coupled with increased expression of *Pik3ap1* and decreased *Lta4h* expression. While LTA4H and its product LTB4 were, to the best of our knowledge, not previously connected to CD8+ T cell proliferation, PIK3AP1-deficiency in CD8+ T cells suppressed clonal expansion and memory generation during *Listeria monocytogenes* infection (18). Our data show that S1PR4 restricts CD8+ T cell proliferation and memory formation in a tumor context, by limiting *Pik3ap1* expression. PIK3AP1 expression by CD8+ T cells appeared to be relevant in patients with colon and mammary tumors. High abundance of PIK3AP1+ CD8+ T cells was negatively correlated with tumor cell proliferation and disease severity, whereas it was positively correlated with improved patient survival. Whether this was associated with the establishment of a memory phenotype remains to be determined. This may be an attractive hypothesis since single cell sequencing of human breast cancer T cells revealed that a CD8+ Trm gene signature to be predictive for improved patient survival (44). The role of CD8+ Trm in colon cancer may also be subject of further studies.

S1PR4-deficient CD8+ T cells were directly linked to reduced tumor growth upon therapy with DXR. This was indicated by the absence of tumor relapse in S1PR4 KO PyMT mice, which was restored after depletion of CD8+ T cells. A recent study showed that SphK1/S1P signaling affected the anti-tumor activity of T cells and co-inhibition of SphK1/PD-1 improved the control of murine melanoma (45). However, in the present study, we only detected a mild synergism of S1PR4 ablation and PD-1 blockade in the PyMT mouse model. This might be due to enhanced expression of type I IFNs in S1PR4 KO PyMT tumors, since it was reported previously that sustained type I IFN expression caused resistance of tumors to anti-PD-1 therapy (17, 46). However, the precise role of IFN signaling in S1PR4-mediated effects on tumor immunity requires further independent validation. Unfortunately, since currently available S1PR4 antagonists show unfavorable pharmacokinetics (unpublished observation), acute in vivo S1PR4 blockade is limited by the availability of suitable tools. Future studies with improved small molecule S1PR4 antagonists will be instrumental in clarifying whether targeting the S1PR4 signaling pathway may be a suitable strategy for the activation of anti-tumor immunity and improvement of cancer therapy.

In conclusion, with this study we show for the first time that S1PR4 signaling inhibits CD8+ T cell abundance through an intrinsic PIK3AP1-/LTA4H-dependent mechanism, which contributed to tumor progression in vivo. However, the impact of other tumor-infiltrating immune cells such as tumor-associated macrophages on the tumor-promoting role of S1PR4 has to be further investigated. Finally, we demonstrate that S1PR4 signaling restricts chemotherapy response through CD8+ T cells and thus propose S1PR4 as potential target to combat cancer.

Materials and methods

Mice

S1PR4 KO mice in the C56BL/6 background were described previously (47). For the polyoma virus middle T oncoprotein (PyMT) model, S1PR4 KO mice or IFNAR1 KO S1PR4 KO mice and their littermate wildtype controls were crossed with mice expressing the PyMT oncogene under the Mouse Mammary Tumor Virus (MMTV) promoter (12), previously bred into a C57BL/6 background to induce mammary carcinoma as described before (36). Only female mice were used for all experiments in the PyMT mouse model. For chemotherapy WT and S1PR4 KO PyMT mice were intraperitoneally (i. p.) injected with 5 mg/kg DXR (Cell pharm GmbH) diluted in sterile 0.9% NaCl once a week for 5 weeks in total. For CD8+ T cell and PD-1 depletion experiments mice were additionally i.p. injected with anti-CD8 (YTS 169.4, BioXCell), anti-PD-1 (4H2, Ono Pharmaceutical) neutralizing antibodies or IgG1 (MOPC-21, BioXCell) or IgG2b (LTF-2, BioXCell) isotype control antibodies diluted in sterile PBS. 250 µg of anti-CD8 and IgG2b antibodies were administrated two times a week for 5 weeks, whereas anti-PD-1 and IgG1 were injected at a concentration of 20 mg/kg at day 0 or 10 mg/kg at days 6, 12, and 18. Tumor size was determined three times a week. For the AOM/DSS model male and female mice of an age between 9 to 14 weeks were used. Mice were injected i.p. with 10 mg/kg AOM (Sigma) at day 0 and day 21 before receiving 0.5% DSS (MP Biomedicals) for the following 5 days in the drinking water. The DSS cycle was repeated at day 47 for additional 5 days. Mouse weight was determined three times a week.

Immunohistochemistry

Investigators were blinded to group allocation during immunohistochemistry. Primary tissue was Zn- (PyMT tumors, lungs) or PFA-fixed (colon) and paraffin-embedded. For

analyzing lung metastasis, lung sections were deparaffinized, stained with Mayer's hemalum (Merck KGaA) and examined under an Axioskop 40 (Zeiss) microscope. Lung panorama pictures were produced using Autostitch software v2.2 (CloudBurst Research Inc). At least 10 independent sections of 4 different lung areas were analyzed. For analyzing colon tumors, colon sections were H&E stained and at least 15 independent sections were analyzed using Aperio ImageScope software (Leica Biosystems). For analyzing murine CD8+ T cells and tissue samples of human colon and invasive breast cancer, provided by the Cooperative Human Tissue Network and the Cancer Diagnosis Program (other investigators may have received specimens from the same subjects), Opal Fluorescent IHC kits (Akoya Biosciences) were used according to the manufacturer's instructions. Primary PyMT tumor sections were stained without antigen retrieval with CD8 antibody (53-6.7, BD Biosciences) or anti-CD45 (D3F8Q, Cell signaling) overnight at 4°C and with corresponding secondary anti-rat IgG-HRP (sc-2006, Santa Cruz Biotechnology) for 1 h at 4°C. For human tissue microarrays prepared paraffin sections were stained with primary antibodies against CD8, KI67, PIK3AP1 (all from Abcam), CD3 (Ventana) and LTA4H (BD). Nuclei were counterstained with DAPI. The BOND RX Automated IHC Research Stainer (Leica Biosystems) was used for staining of human tissue microarrays. Samples were acquired at 20× magnification using the Vectra3 automated quantitative pathology imaging system (Akoya Biosciences). InForm v2.1 (Akoya Biosciences) was used to quantify the percentage of LTA4H-, PIK3AP1-expressing CD8+ T cells and KI67+ cells in human colon and invasive breast cancer cores. Cancer cores were evaluated based on tissue integrity and quality after staining. Based on these criteria, 145 individual cores were suitable for analysis.

Flow cytometry and FACS sorting

Samples were acquired with a LSRII/Fortessa flow cytometer (BD Biosciences) and analyzed using FlowJo software Vx (Treestar). All antibodies and secondary reagents were titrated to determine optimal concentrations. CompBeads (BD Biosciences) were used for single-color compensation to create multi-color compensation matrices. For gating, fluorescence minus one (FMO) controls were used. The instrument calibration was controlled daily using Cytometer Setup and Tracking beads (BD Biosciences). Single cell suspensions were created using the Tumor and Lamina Propria dissociation kit (Miltenyi) and the GentleMACS dissociator (Miltenyi) using standard protocols. For details on antibodies and staining procedures see supplemental experimental procedures. Data were analyzed using FlowJo V10.6.1 including the tSNE plug-in.

MDSC suppression assay

For MDSC differentiation femurs and tibias of 10 to 12 week old WT and S1PR4 KO mice were flushed with PBS and cells were filtered through a 70 µm syringe falcon (BD Biosciences) before FACS sorting for granulocyte/monocyte progenitors (GMPs). For FACS sorting of GMPs bone marrow cells were pre-incubated with anti-CD16/32-PerCP-Cy5.5 (BD Biosciences, 2.4G2) before stained with anti-B220-VioBlue (Miltenyi, RA3-6B2), anti-CD117-APC-eFluor780 (eBioscience, ACK2), anti-CD34-PE (Immunotools, MEC14.7) and anti-MHCII-PE-Cy7. GMPs were classified as B220- MHCII- CD16/32+ CD34+ CD117+ before seeded in 24-well ultra-low attachment plates (Corning Costar) in a density of 6 x 10^4 per well and differentiated to MDSCs with 20 ng/ml GM-CSF and 10 ng/ml IL-4 for 5 days. At day 5 splenocytes of WT mice were pre-labeled with Cell Proliferation Dye eFluor 670 (eBioscience) according to manufacturer's instructions. Pre-labeled splenocytes were added in indicated ratios to 2 x 10^4 MDSCs and co-cultured for additional 3 days before cell proliferation was

determined by FACS. For details on antibodies and staining procedures of Arg1+ gMDSCs and mMDSCs in PyMT tumors and colons see supplemental experimental procedures.

Quantitative PCR

RNA from CD8+ T cells was isolated using the RNeasy Micro Kit (Qiagen) followed by cDNA transcription with the SensiScript cDNA synthesis kit (Qiagen). The murine primer sequences are shown in the supplemental experimental procedure section. The results were analyzed using Gene Expression Macro (Bio-Rad). *Rps27a* served as the internal control.

Chemokine quantification

To determine the levels of 13 different chemokines in tumor supernatants of WT and S1PR4 KO PyMT mice the LEGENDplex™ mouse proinflammatory chemokine panel was used (Biolegend) according to the manufacturer's instructions. Samples were acquired by flow cytometry and analyzed using FlowJo V10.

Cell migration

For the Boyden chamber assays, 3 x 10^6 total splenocytes (in serum-free RPMI 1640 medium) were added to transwell inserts (5 µm, Corning Costar) and allowed to migrate towards extracellular fluid from WT or KO PyMT tumors (1:10 dilution) in the lower compartment for 2 h. Migrated and non-migrated cells were characterized by flow cytometry with Flow Cytometry Absolute Count Standard™ (BangsLabs) as an internal counting standard. The percentage of migration was determined as the ratio of migrated vs. non-migrated cells.

T cell proliferation assay

CD8+ T cells were isolated from murine spleens using a murine CD8+ T cell Isolation Kit (Stemcell Technologies) and cultured in T cell medium (RPMI 1640, supplemented with 5 mM glutamine, 100 U/ml penicillin, 100 µg/ml streptomycin, 10% heat-inactivated FCS, 1% nonessential and essential aminoacids, 1% sodiumpyruvate and 1% HEPES). 3 x 10^5 CD8+ T cells were pre-treated with or without 5 µM SC 57461A (Sigma-Aldrich), 5 µM AIP (Tocris) or 0.5 µM Ly294002 (Sigma-Aldrich) followed by stimulation with mouse T activator CD3/CD28 Dynabeads (Thermo Fisher Scientific) before being cultured for 10 to 14 days, with the addition of 50 µM β-mercaptoethanol daily and 10 ng of murine IL-2 (Peprotech) at days 0, 2 and 4. For S1PR4 agonist or antagonist studies isolated CD8+ T cells were pre-treated with 200 nM S1PR4 agonist Cym 50308 or antagonist 200 nM Cym 50358 (both from Tocris) for 24 h before activation and with or without addition of 5 µM Arm1 or 20 µM PGP (both from Cayman Chemical). Cym 50308 and Cym 50358 were added daily. LTB4 protein levels were determined from harvested supernatants of cultured CD8+ T cells one day after activation by ELISA (R&D Systems).

T cell – 3D spheroid co-culture

For the PyMT spheroid co-culture CD326+ CD45- PyMT cells were initially isolated from a WT PyMT tumor and cultured in RPMI 1640, supplemented with 5 mM glutamine, 100 U/ml penicillin, 100 µg/ml streptomycin as well as 10% heat-inactivated FCS and were maintained at 37°C in a humidified atmosphere with 5% CO2. Spheroids generated from PyMT cells were initiated using 1 x 10^4 cells/ml and were cultured in cell-repellent 96-well plates (Greiner Bio-One GmbH) with a final concentration of 1.5% growth factor reduced Matrigel (Corning Costar) for 12 days. For PyMT spheroid CD8+ T cell co-cultures media was changed prior to the addition of 3 x 10^4 CD8+ T cells per

spheroid. Prior addition, CD8+ T cells were pre-treated and pre-activated as described above followed by two washing steps. CD8+ T cell – PyMT spheroid co-cultures were maintained for 10 days in T cell medium. For human PBMC/MCF-7 spheroid co-cultures media of spheroids were changed prior to PBMC addition. PBMCs were either left untreated or stimulated with 10 ng/ml LPS and 100 U/ml IFNγ with or without addition of 200 nM S1PR4 agonist Cym50308 or S1PR4 antagonist Cym50358 (both from Tocris) for 30 min. PBMCs were subsequently co-cultured with MCF-7 tumor spheroids for 6 days, with re-adding of S1PR4 agonist and antagonist at day 3. Spheroid size was acquired with a Carl Zeiss Axiovert microscope and diameters were determined using AxioVision 40 software (Carl Zeiss AG).

Next generation sequencing

PyMT tumors and total colons were isolated and dissociated using the murine tumor and lamina propria dissociation kit (Miltenyi). For sequencing of PyMT CD8+ T cells, cells were isolated by FACS-sorting as described above. For sequencing of total colon, tissue was snap-frozen. RNA from isolated CD8+ T cells and total colon tissue was extracted using the RNeasy Micro Kit (Qiagen). For sequencing of PyMT CD8+ T cells RNA quality was evaluated by an Agilent 2100 Bioanalyzer using a RNA 6000 Pico Chip (Agilent Technologies), followed by quantification with a Qubit HS RNA Assay Kit (Thermo Fisher Scientific). 10 ng of RNA was taken for library preparation using the SMARTer Stranded Total RNA-Seq Kit v2-Pico Input (Takara Bio). Quantity and quality of the complementary DNA (cDNA) libraries were evaluated by Qubit ds DNA HS Assay Kit (Thermo Fisher Scientific) and Agilent DNA High Sensitivity DNA Chip (Agilent Technologies), respectively. Libraries for PyMT CD8+ T cells were sequenced (single-end, 75 cycles) using the High Output Kit v2 on a NextSeq 500 sequencer (Illumina). NGS data analysis was performed using the SeqBox ecosystem. Briefly,

after adapter trimming with skewer, reads were mapped to the murine reference genome (mm10) using STAR. Gene level quantification by RSEM preceded the differential expression analysis by DESeq2. CDNA library preparation and sequencing of total colons was performed by the DKFZ Genomics & Proteomics Core Facility. NGS data analysis was performed as described previously (48). Reads were mapped to the murine reference genome (mm9). The complete dataset is available at GEO: GSE152032.

Gene knockdown in primary T cells

1 x 10^6 WT or S1PR4 KO CD8+ T cells were incubated with 1 µM of Accell SMARTpool PIK3AP1 or non-targeting control siRNA (both from Dharmacon) in T cell medium supplemented with 2% FCS for 48h before FCS was re-added to a final concentration of 10%. After additional 24h of incubation CD8+ T cells were activated with mouse T activator CD3/CD28 Dynabeads (Thermo Fisher Scientific) for 30 min and stained intracellularly for anti-phospho-AKT (Ser473)-PE (Cell signaling, D9E). For intracellular staining CD8+ T cells were harvested and incubated with 4% PFA for 15 min before Fixation/Permeabilization Solution Kit (BD Biosciences) was used according to manufacturer's instructions.

Analysis of publicly available human mammary carcinoma datasets

The TCGA colon adenocarcinoma data set (27) and the METABRIC datasets (26) were downloaded from cBioPortal for Cancer Genomics (http://www.cbioportal.org) including associated clinical data. An *in silico* S1P ratio was generated by comparing mean expression of S1P generating, versus S1P degrading enzymes (mean expression (SPHK1 + SPHK2) / mean expression (SGPL1 + SGPP1 + SGPP2 +

PPAP2B)) and compared with patient survival and the expression of CD8A and CD103 in the individual datasets.

GSEA analysis

Differentially expressed genes between WT and S1PR4 KO CD8+ T cells were used as an input to analyze gene sets in the Molecular Signatures Database using GSEA 4.0.2 via the Gene Pattern Platform.

Statistics

Unless otherwise stated, data are presented as means ± SEM. Statistically significant differences between groups were calculated using two-tailed Student's t-test or two-way ANOVA with Bonferroni's post-correction for analysis of parametric data. A D'Agostino and Pearson omnibus normality test was performed to test whether the data followed a Gaussian distribution. Parametric or non-parametric tests were applied accordingly. A P Value less than 0.05 was considered significant.

Study approval

Mouse care and experiments involving mice were approved by and followed the guidelines of the Hessian animal care and use committee (FU/1010, FU/1123, FU/1169, FU/1191).

Author contributions

CO, and AW conceptualized and designed research, CO, BR, and AW developed methodology. CO, ESF, MB, RS, AF, BR, and AW performed experiments and acquired data, CO, ESF, and AW analyzed and interpreted results, D.S., FG, KT, and BB provided technical and material support, BB, and AW supervised research, and all authors participated in writing the manuscript.

Acknowledgements

The authors thank Praveen Mathoor and Margarete Mijatovic for excellent technical assistance.

Grant support

This work was supported by Deutsche Krebshilfe (110637, 70112451), Deutsche Forschungsgemeinschaft (FOR 2438, TP3 and 8; SFB 1039, TP B04 and B06, GRK 2336, TP1 and 6), Wilhelm-Sander Foundation (2019.082.01) and the LOEWE Center Frankfurt Cancer Institute (FCI) funded by the Hessen State Ministry for Higher Education, Research and the Arts [III L 5 - 519/03/03.001 - (0015)].

References

1. Liu S, Lachapelle J, Leung S, Gao D, Foulkes WD, and Nielsen TO. CD8+ lymphocyte infiltration is an independent favorable prognostic indicator in basal-like breast cancer. *Breast cancer research : BCR.* 2012;14(2):R48.
2. Pages F, Kirilovsky A, Mlecnik B, Asslaber M, Tosolini M, Bindea G, Lagorce C, Wind P, Marliot F, Bruneval P, et al. In situ cytotoxic and memory T cells predict outcome in patients with early-stage colorectal cancer. *Journal of clinical oncology : official journal of the American Society of Clinical Oncology.* 2009;27(35):5944-51.
3. Topalian SL, Drake CG, and Pardoll DM. Immune checkpoint blockade: a common denominator approach to cancer therapy. *Cancer Cell.* 2015;27(4):450-61.
4. Rivera J, Proia RL, and Olivera A. The alliance of sphingosine-1-phosphate and its receptors in immunity. *Nat Rev Immunol.* 2008;8(10):753-63.
5. Weigert A, Johann AM, von Knethen A, Schmidt H, Geisslinger G, and Brune B. Apoptotic cells promote macrophage survival by releasing the antiapoptotic mediator sphingosine-1-phosphate. *Blood.* 2006;108(5):1635-42.
6. Gude DR, Alvarez SE, Paugh SW, Mitra P, Yu J, Griffiths R, Barbour SE, Milstien S, and Spiegel S. Apoptosis induces expression of sphingosine kinase 1 to release sphingosine-1-phosphate as a "come-and-get-me" signal. *Faseb J.* 2008;22(8):2629-38.
7. Pyne NJ, and Pyne S. Sphingosine 1-phosphate and cancer. *Nat Rev Cancer.* 2010;10(7):489-503.
8. Aoyagi T, Nagahashi M, Yamada A, and Takabe K. The role of sphingosine-1-phosphate in breast cancer tumor-induced lymphangiogenesis. *Lymphat Res Biol.* 2012;10(3):97-106.
9. Olesch C, Ringel C, Brune B, and Weigert A. Beyond Immune Cell Migration: The Emerging Role of the Sphingosine-1-phosphate Receptor S1PR4 as a Modulator of Innate Immune Cell Activation. *Mediators of inflammation.* 2017;2017(6059203.
10. Dillmann C, Ringel C, Ringleb J, Mora J, Olesch C, Fink AF, Roberts E, Brune B, and Weigert A. S1PR4 Signaling Attenuates ILT 7 Internalization To Limit IFN-alpha Production by Human Plasmacytoid Dendritic Cells. *J Immunol.* 2016;196(4):1579-90.
11. Sekar D, Hahn C, Brune B, Roberts E, and Weigert A. Apoptotic tumor cells induce IL-27 release from human DCs to activate Treg cells that express CD69 and attenuate cytotoxicity. *Eur J Immunol.* 2012;42(6):1585-98.
12. Guy CT, Cardiff RD, and Muller WJ. Induction of mammary tumors by expression of polyomavirus middle T oncogene: a transgenic mouse model for metastatic disease. *Mol Cell Biol.* 1992;12(3):954-61.
13. Lin EY, Jones JG, Li P, Zhu L, Whitney KD, Muller WJ, and Pollard JW. Progression to malignancy in the polyoma middle T oncoprotein mouse breast cancer model provides a reliable model for human diseases. *Am J Pathol.* 2003;163(5):2113-26.
14. Bates JP, Derakhshandeh R, Jones L, and Webb TJ. Mechanisms of immune evasion in breast cancer. *BMC cancer.* 2018;18(1):556.
15. Sekar D, Govene L, Del Rio ML, Sirait-Fischer E, Fink AF, Brune B, Rodriguez-Barbosa JI, and Weigert A. Downregulation of BTLA on NKT Cells Promotes

Tumor Immune Control in a Mouse Model of Mammary Carcinoma. *International journal of molecular sciences.* 2018;19(3).
16. Wherry EJ, and Kurachi M. Molecular and cellular insights into T cell exhaustion. *Nature reviews Immunology.* 2015;15(8):486-99.
17. Garcia-Diaz A, Shin DS, Moreno BH, Saco J, Escuin-Ordinas H, Rodriguez GA, Zaretsky JM, Sun L, Hugo W, Wang X, et al. Interferon Receptor Signaling Pathways Regulating PD-L1 and PD-L2 Expression. *Cell reports.* 2019;29(11):3766.
18. Singh MD, Ni M, and Sullivan JM. B cell adaptor for PI3-kinase (BCAP) modulates CD8(+) effector and memory T cell differentiation. 2018;215(9):2429-43.
19. Lin MY, Zal T, Ch'en IL, Gascoigne NR, and Hedrick SM. A pivotal role for the multifunctional calcium/calmodulin-dependent protein kinase II in T cells: from activation to unresponsiveness. *Journal of immunology (Baltimore, Md : 1950).* 2005;174(9):5583-92.
20. Wang YY, Zhao R, and Zhe H. The emerging role of CaMKII in cancer. *Oncotarget.* 2015;6(14):11725-34.
21. Okada T, Maeda A, Iwamatsu A, Gotoh K, and Kurosaki T. BCAP: the tyrosine kinase substrate that connects B cell receptor to phosphoinositide 3-kinase activation. *Immunity.* 2000;13(6):817-27.
22. Tang F, Sally B, Lesko K, Discepolo V, Abadie V, Ciszewski C, Semrad C, Guandalini S, Kupfer SS, and Jabri B. Cysteinyl leukotrienes mediate lymphokine killer activity induced by NKG2D and IL-15 in cytotoxic T cells during celiac disease. *J Exp Med.* 2015;212(10):1487-95.
23. Savari S, Vinnakota K, Zhang Y, and Sjölander A. Cysteinyl leukotrienes and their receptors: bridging inflammation and colorectal cancer. *World journal of gastroenterology.* 2014;20(4):968-77.
24. Appiah-Kubi P, and Soliman ME. Dual anti-inflammatory and selective inhibition mechanism of leukotriene A4 hydrolase/aminopeptidase: insights from comparative molecular dynamics and binding free energy analyses. *Journal of biomolecular structure & dynamics.* 2016;34(11):2418-33.
25. Atluru D, and Goodwin JS. Leukotriene B4 causes proliferation of interleukin 2-dependent T cells in the presence of suboptimal levels of interleukin 2. *Cellular immunology.* 1986;99(2):444-52.
26. Curtis C, Shah SP, Chin SF, Turashvili G, Rueda OM, Dunning MJ, Speed D, Lynch AG, Samarajiwa S, Yuan Y, et al. The genomic and transcriptomic architecture of 2,000 breast tumours reveals novel subgroups. *Nature.* 2012;486(7403):346-52.
27. Hoadley KA, Yau C, Hinoue T, Wolf DM, Lazar AJ, Drill E, Shen R, Taylor AM, Cherniack AD, Thorsson V, et al. Cell-of-Origin Patterns Dominate the Molecular Classification of 10,000 Tumors from 33 Types of Cancer. *Cell.* 2018;173(2):291-304 e6.
28. Tsuchida J, and Nagahashi M. Clinical Impact of Sphingosine-1-Phosphate in Breast Cancer. 2017;2017(2076239.
29. Ogretmen B. Sphingolipid metabolism in cancer signalling and therapy. *Nat Rev Cancer.* 2018;18(1):33-50.
30. Pal SK, Drabkin HA, Reeves JA, Hainsworth JD, Hazel SE, Paggiarino DA, Wojciak J, Woodnutt G, and Bhatt RS. A phase 2 study of the sphingosine-1-phosphate antibody sonepcizumab in patients with metastatic renal cell carcinoma. *Cancer.* 2017;123(4):576-82.

31. Britten CD, Garrett-Mayer E, Chin SH, Shirai K, Ogretmen B, Bentz TA, Brisendine A, Anderton K, Cusack SL, Maines LW, et al. A Phase I Study of ABC294640, a First-in-Class Sphingosine Kinase-2 Inhibitor, in Patients with Advanced Solid Tumors. *Clin Cancer Res.* 2017;23(16):4642-50.
32. Deng J, Liu Y, Lee H, Herrmann A, Zhang W, Zhang C, Shen S, Priceman SJ, Kujawski M, Pal SK, et al. S1PR1-STAT3 signaling is crucial for myeloid cell colonization at future metastatic sites. *Cancer Cell.* 2012;21(5):642-54.
33. Lee H, Deng J, Kujawski M, Yang C, Liu Y, Herrmann A, Kortylewski M, Horne D, Somlo G, Forman S, et al. STAT3-induced S1PR1 expression is crucial for persistent STAT3 activation in tumors. *Nat Med.* 2010;16(12):1421-8.
34. Nagahashi M, Yamada A, Katsuta E, Aoyagi T, Huang WC, Terracina KP, Hait NC, Allegood JC, Tsuchida J, Yuza K, et al. Targeting the SphK1/S1P/S1PR1 axis that links obesity, chronic inflammation and breast cancer metastasis. *Cancer Res.* 2018.
35. Priceman SJ, Shen S, Wang L, Deng J, Yue C, Kujawski M, and Yu H. S1PR1 is crucial for accumulation of regulatory T cells in tumors via STAT3. *Cell Rep.* 2014;6(6):992-9.
36. Weichand B, Popp R, Dziumbla S, Mora J, Strack E, Elwakeel E, Frank AC, Scholich K, Pierre S, Syed SN, et al. S1PR1 on tumor-associated macrophages promotes lymphangiogenesis and metastasis via NLRP3/IL-1beta. *J Exp Med.* 2017;214(9):2695-713.
37. Du W, Takuwa N, Yoshioka K, Okamoto Y, Gonda K, Sugihara K, Fukamizu A, Asano M, and Takuwa Y. S1P(2), the G protein-coupled receptor for sphingosine-1-phosphate, negatively regulates tumor angiogenesis and tumor growth in vivo in mice. *Cancer Res.* 2010;70(2):772-81.
38. Garris CS, Blaho VA, Hla T, and Han MH. Sphingosine-1-phosphate receptor 1 signalling in T cells: trafficking and beyond. *Immunology.* 2014;142(3):347-53.
39. Gaengel K, Niaudet C, Hagikura K, Lavina B, Muhl L, Hofmann JJ, Ebarasi L, Nystrom S, Rymo S, Chen LL, et al. The sphingosine-1-phosphate receptor S1PR1 restricts sprouting angiogenesis by regulating the interplay between VE-cadherin and VEGFR2. *Dev Cell.* 2012;23(3):587-99.
40. Cohen JA, Barkhof F, Comi G, Hartung HP, Khatri BO, Montalban X, Pelletier J, Capra R, Gallo P, Izquierdo G, et al. Oral fingolimod or intramuscular interferon for relapsing multiple sclerosis. *N Engl J Med.* 2010;362(5):402-15.
41. Xiong Y, Piao W, Brinkman CC, Li L, Kulinski JM, Olivera A, Cartier A, Hla T, Hippen KL, Blazar BR, et al. CD4 T cell sphingosine 1-phosphate receptor (S1PR)1 and S1PR4 and endothelial S1PR2 regulate afferent lymphatic migration. *Sci Immunol.* 2019;4(33).
42. Dillmann C, Mora J, Olesch C, Brune B, and Weigert A. S1PR4 is required for plasmacytoid dendritic cell differentiation. *Biol Chem.* 2015.
43. Schulze T, Golfier S, Tabeling C, Rabel K, Graler MH, Witzenrath M, and Lipp M. Sphingosine-1-phospate receptor 4 (S1P(4)) deficiency profoundly affects dendritic cell function and TH17-cell differentiation in a murine model. *FASEB journal : official publication of the Federation of American Societies for Experimental Biology.* 2011;25(11):4024-36.
44. Savas P, Virassamy B, Ye C, Salim A, Mintoff CP, Caramia F, Salgado R, Byrne DJ, Teo ZL, Dushyanthen S, et al. Single-cell profiling of breast cancer T cells reveals a tissue-resident memory subset associated with improved prognosis. 2018;24(7):986-93.
45. Chakraborty P, Vaena SG, Thyagarajan K, Chatterjee S, Al-Khami A, Selvam SP, Nguyen H, Kang I, Wyatt MW, Baliga U, et al. Pro-Survival Lipid

Sphingosine-1-Phosphate Metabolically Programs T Cells to Limit Anti-tumor Activity. *Cell reports.* 2019;28(7):1879-93.e7.
46. Jacquelot N, Yamazaki T, and Roberti MP. Sustained Type I interferon signaling as a mechanism of resistance to PD-1 blockade. 2019;29(10):846-61.
47. Dillmann C, Mora J, Olesch C, Brune B, and Weigert A. S1PR4 is required for plasmacytoid dendritic cell differentiation. *Biological chemistry.* 2015;396(6-7):775-82.
48. Michels BE, and Mosa MH. Human colon organoids reveal distinct physiologic and oncogenic Wnt responses. 2019;216(3):704-20.

Figures and figure legends

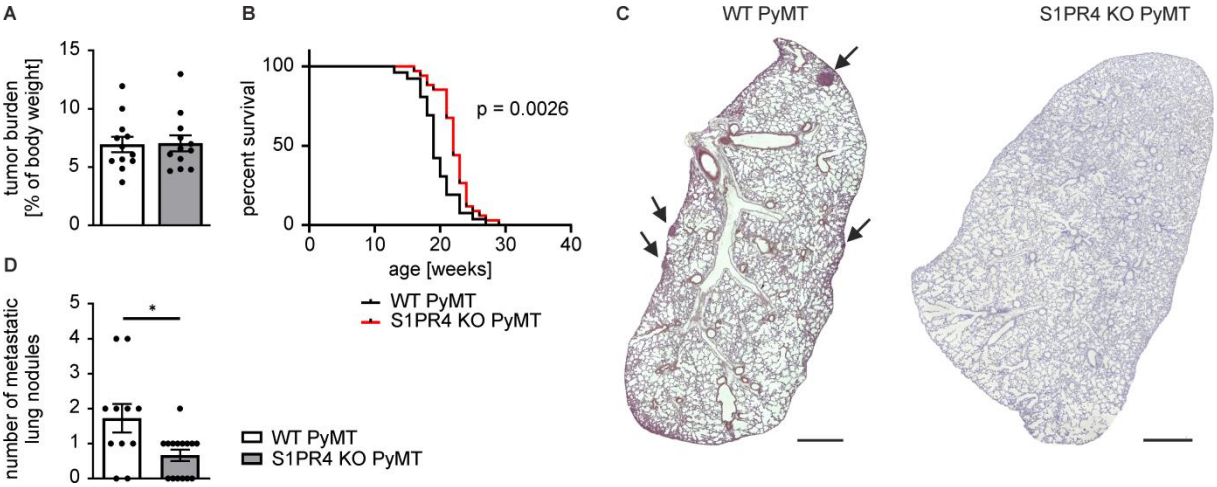

Figure 1 S1PR4 ablation delays mammary tumor progression and reduces lung metastasis. S1PR4 KO and WT mice were crossed into the polyoma middle T oncogene (PyMT) background. (A) Tumor burden at the endpoint (once one tumor reached a diameter of ~ 1.5 cm). (B) Kaplan-Meier curve showing survival of WT (n = 26) and S1PR4 KO PyMT mice (n = 34) until the endpoint. (C) Representative sections of lung lobes stained with Mayer's hemalum. Arrows indicate metastases. Scale bars represent 1 mm. (D) Number of metastatic lung nodules in WT (n = 11) and S1PR4 KO PyMT mice (n = 15) at the endpoint. Means ± SEM; two-tailed Student's t test; *p<0.05, **p<0.01.

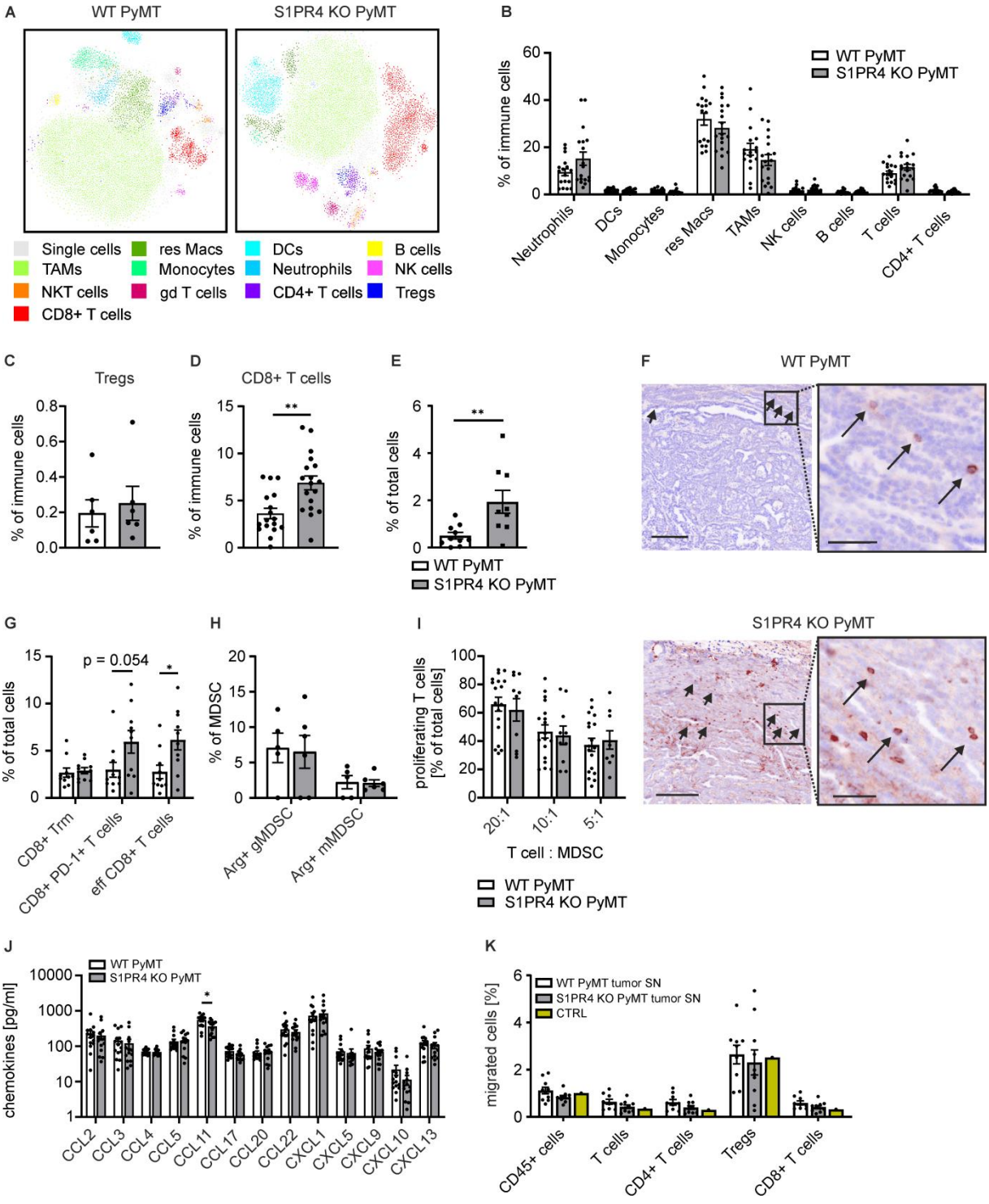

Figure 2 S1PR4 ablation promotes CD8+ T cell expansion in mammary tumors. (A) Representative tSNE plots show differences in immune cell infiltrates at the endpoint. (B-D) Relative amounts of immune cell populations (B), FoxP3+ Tregs (C) and CD8+ T cells (D) in PyMT tumors of WT (n = 17) and KO (n = 18) mice analyzed by FACS. (E, F) Sections from PyMT tumors were stained for CD8+ cytotoxic T cells. (E) Quantification of CD8+ T cells as percentage of total cells (WT: n = 10, KO: n = 9) and (F) representative sections stained for CD8 (brown) and DAPI (blue; nuclei). Scale bars represent 200 µm; scale bars of magnified areas represent 50 µm. (G) Relative amounts of Trm (CD103+), exhausted (PD-1+) and effector CD8+ T cells (CD49a-CD103-) in tumors (n = 10) determined by FACS. (H) Relative amounts of gMDSCs

(CD11b+ Ly6G high Ly6C low) and mMDSCs (CD11b+ Ly6G low Ly6C high) in PyMT tumors (WT: n = 5, KO: n = 6) expressing arginase 1 (Arg1) determined by FACS. (I) Relative amounts of proliferating T cells upon co-culture with WT (n = 18) and S1PR4 KO (n = 10) MDSCs in different ratios determined by FACS. (J) Chemokine levels in WT (n = 15) and S1PR4 KO PyMT (n = 14) tumors determined by LEGENDplex. (K) Splenocytes of WT mice in the upper well of a modified Boyden chamber were allowed to migrate towards extracellular fluid from WT and S1PR4 KO PyMT tumors (n = 10). Migrated cell populations were analyzed by FACS. Heat-inactivated FCS served as control. Means ± SEM; two-tailed Student’s t test (D, E, G, J), two-way ANOVA with Sidak's correction (K); *p<0.05, **p<0.01.

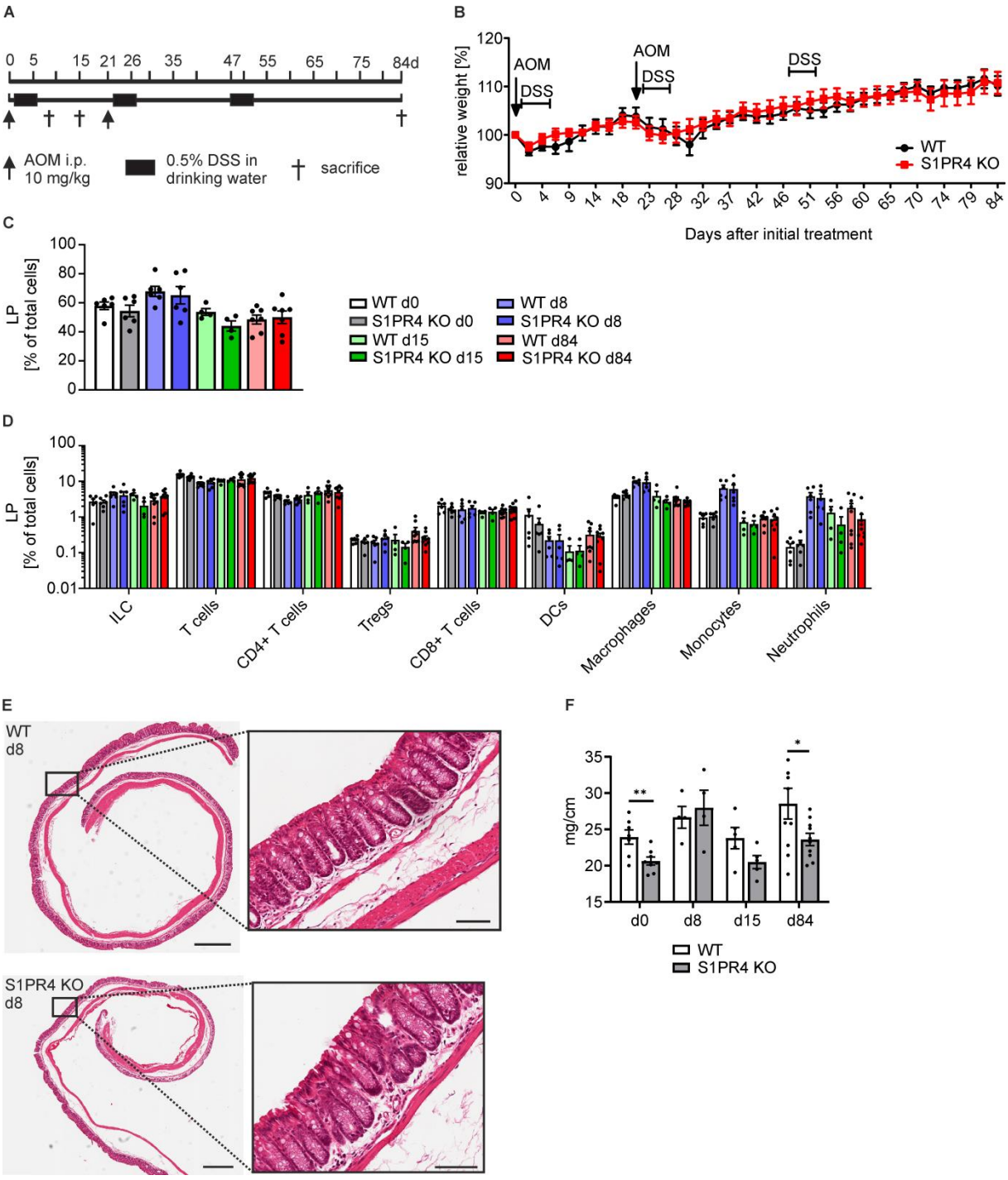

Figure 3 S1PR4 signaling does not affect initial inflammation in the AOM/DSS model of colitis-associated cancer. (A) Experimental outline of the AOM/DSS model applied to WT and S1PR4 KO mice. (B) Weight of AOM/DSS-treated WT and S1PR4 KO mice as percentage of weight at the initiation of treatment (n = 9). (C, D) Relative amounts of CD45+ leukocytes (C) and immune cell populations (D) in the lamina propria of WT and S1PR4 KO mice at day 0 (n = 6), day 8 (n = 8), day 15 (n = 4) and day 84 (n = 9) analyzed by flow cytometry. (E) Representative pictures of WT and S1PR4 KO AOM/DSS-treated colon tissue at day 8 stained with hematoxylin and eosin. Scale bars represent 1 mm; scale bars of magnified areas represent 100 µm. (F) Colon weight to length ratio determined for WT and KO AOM/DSS-treated mice at

days 0 (WT: n = 7, KO: n = 8), 8 (n = 4), 15 (n = 5), and 84 (n = 10). Means ± SEM; two-tailed Student’s t test; *p<0.05.

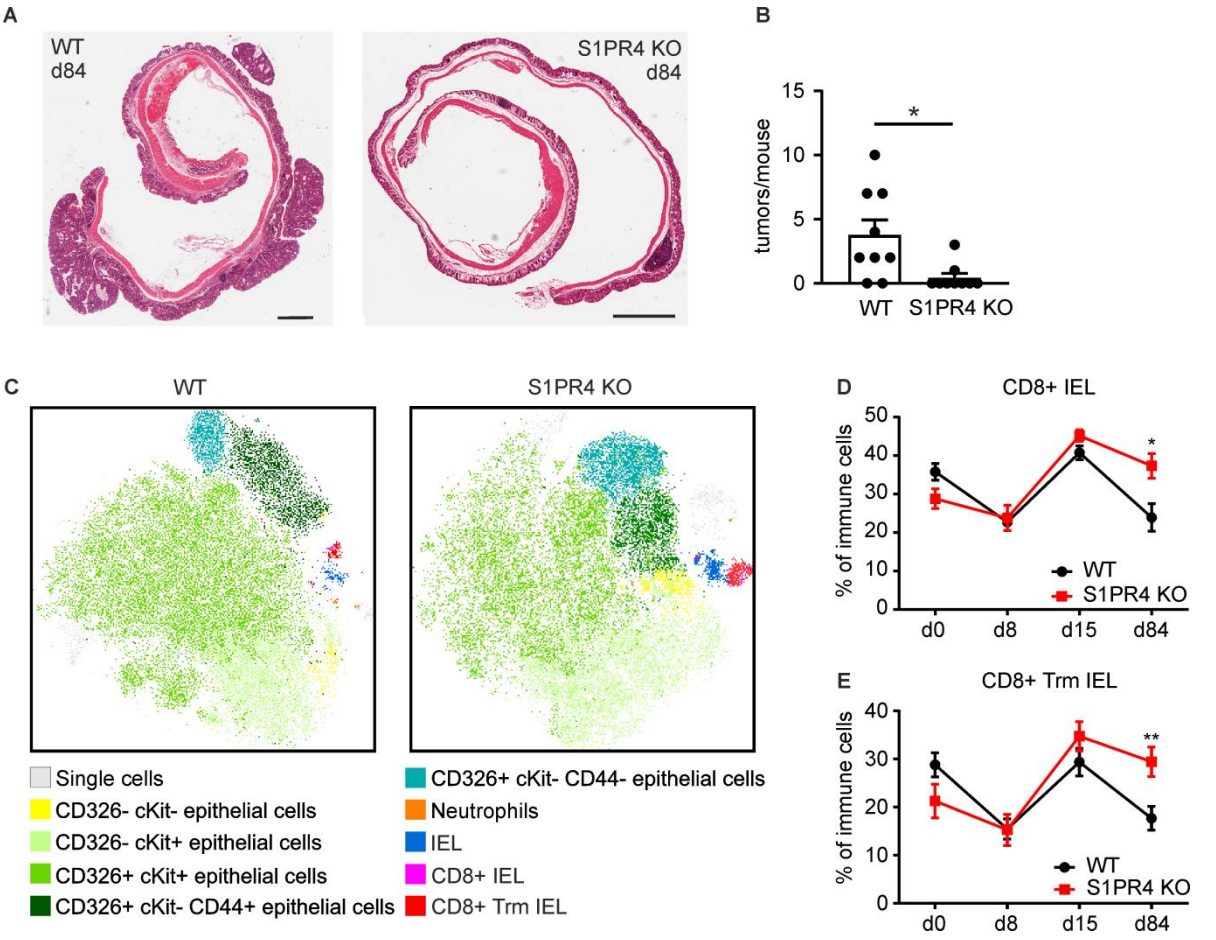

Figure 4 S1PR4 ablation restricts tumor formation of colitis-associated cancer and induces epithelial CD8+ T cell expansion. (A) Representative images of WT and S1PR4 KO AOM/DSS-treated colons at day 84 stained with hematoxylin and eosin. Scale bars represent 1 mm. (B) Number of tumors per mouse for WT and S1PR4 KO mice (n = 9) at day 84 after treatment with AOM/DSS. (C) Representative tSNE plots showing the composition of the epithelial layer from WT and S1PR4 KO colons at day 84. (D, E) Relative amounts of CD8+ IEL (D) and CD8+ Trm IEL (E) within the epithelial layer of WT and S1PR4 KO mice at day 0 (n = 6), day 8 (n = 8), day 15 (n = 4) and day 84 (n = 9) analyzed by flow cytometry. Means ± SEM; two-tailed Student's t test; *p<0.05, **p<0.01.

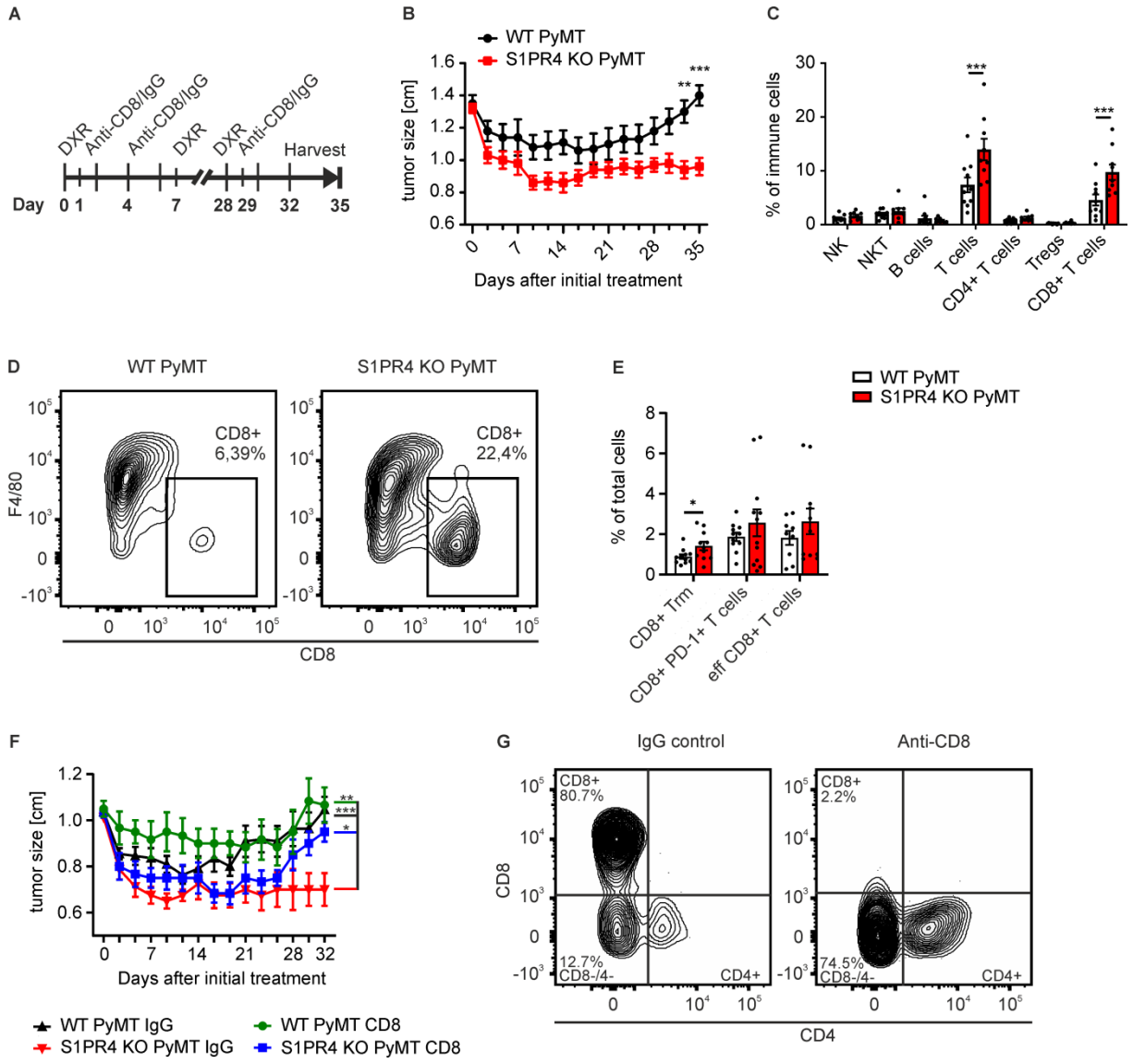

Figure 5 S1PR4 ablation improves response to chemotherapy through CD8+ T cells. (A) WT and S1PR4 KO PyMT mice were treated with 5 mg/kg DXR once a week without (B-E) or with CD8 depleting antibodies (F, G). (B) Tumor size kinetics in DXR-treated PyMT mice (n = 10). (C) Relative amounts of lymphocyte subsets in PyMT tumors of WT (n = 10) and S1PR4 KO (n = 9) mice after 5 weeks of DXR treatment. (D) Representative FACS plots showing percentage of CD8+ T cells in PyMT tumors. (E) Relative amounts of Trm (CD103+), exhausted (PD-1+) and effector CD8+ T cells (CD49a- CD103-) in DXR-treated WT (n = 11) and KO (n = 12) PyMT tumors determined by FACS. (F) Tumor size kinetics in DXR and anti-CD8 antibody (n = 6) or IgG control antibody (WT: n = 11, S1PR4 KO: n = 8) treated PyMT mice. (G) Representative FACS plots showing percentage of CD8+ and CD8/4 double negative T cells in IgG or anti-CD8 treated WT PyMT tumors. Means ± SEM; two-way ANOVA with Sidak's correction (B, C, F), two-tailed Student's t test (E); *p<0.05, **p<0.01, ***p<0.001.

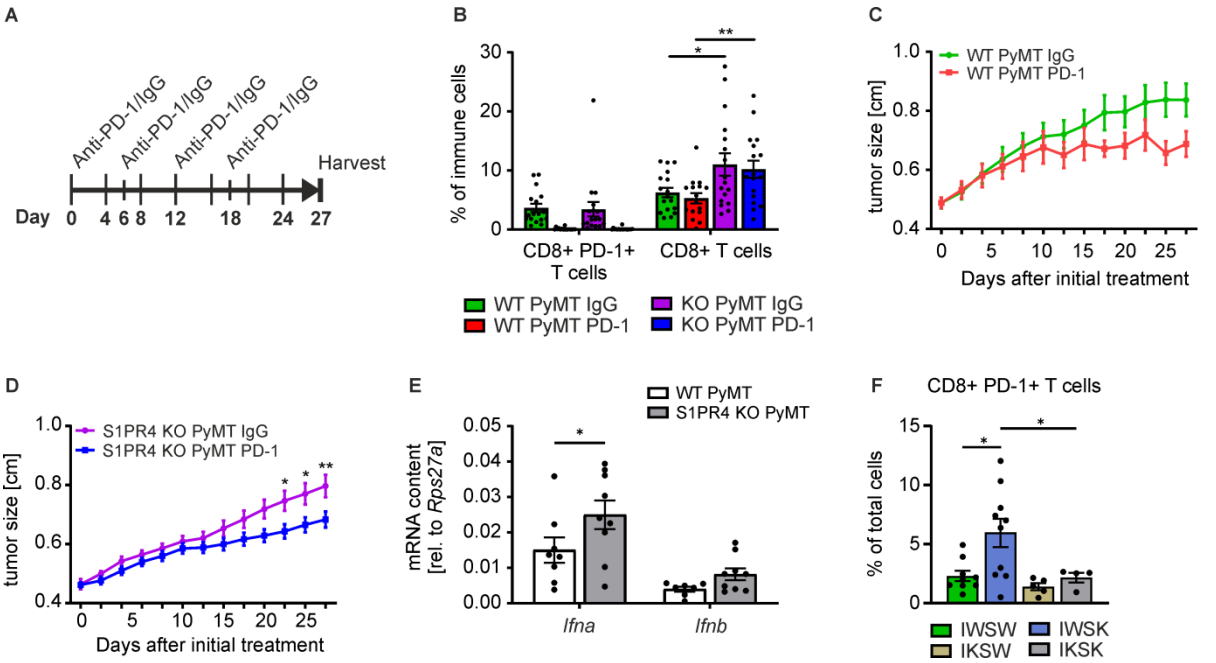

Figure 6 S1PR4 ablation increases CD8+ PD-1+ T cell abundance and moderately improves anti-PD-1 therapy. (A-D) WT and S1PR4 KO PyMT mice were treated with either anti-PD-1 or IgG isotype control antibodies (n = 17 each) on day 0, 6, 12 and 18 once the first tumor reached a size of 0.6 cm in diameter. Tumors were harvested at day 27. (A) Experimental outline. (B) Relative amounts of CD8+ PD-1+ and total CD8+ T cells infiltrated into PyMT tumors (n = 17) four weeks after treatment start. (C, D) Tumor size kinetics of treated WT (C) and S1PR4 KO (n = 16) PyMT mice (D). (E) *Ifna* and *Ifnb* mRNA expression in WT (n = 8) and S1PR4 KO (n = 9) PyMT tumors determined by qPCR. (F) Relative amounts of exhausted CD8+ PD-1+ T cells in PyMT tumors of IFNAR1 WT S1PR4 WT (IWSW, n = 9), IFNAR1 WT S1PR4 KO (IWSK, n = 10), IFNAR1 KO S1PR4 WT (IKSW, n = 5) and IFNAR1 KO S1PR4 KO (IKSK, n = 4) once one tumor reached a size of ~ 1.5 cm. Means ± SEM; two-way ANOVA with Sidak's correction (B, D), one-way ANOVA with Sidak's correction (F); *p<0.05, **p<0.01.

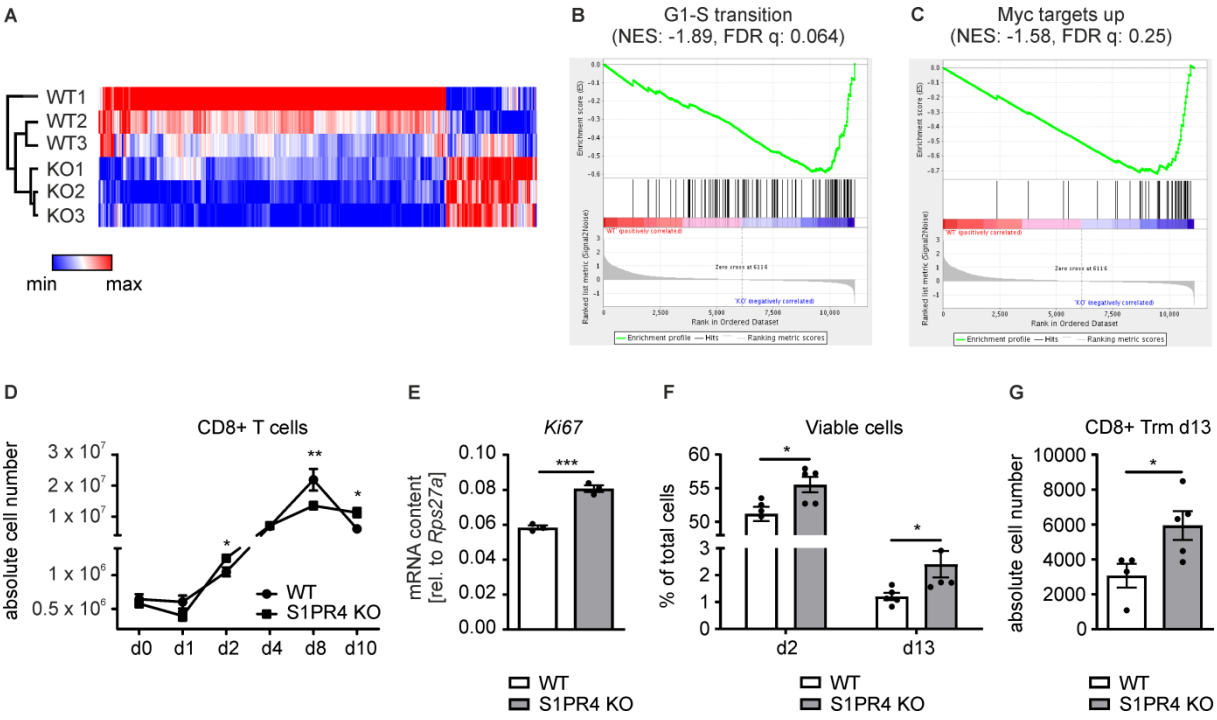

Figure 7 S1PR4 ablation enhances CD8+ T cell proliferation and survival. (A) Unsupervised hierarchical cluster analysis of FACS-sorted WT and S1PR4 KO PyMT CD8+ T cell gene expression profiles (top 300 differentially expressed genes). (B, C) Representative gene set enrichment plots of gene sets enriched in KO PyMT CD8+ T cells. (D) Absolute cell number of splenic WT and S1PR4 KO CD8+ T cells after activation at days 0, 2 and 4. One representative experiment of 3 independent biological replicates is shown, which was repeated five times with similar outcomes. (E) *Ki67* expression of WT and S1PR4 KO CD8+ T cells (n = 3) at day 2 determined by qPCR. (F) Relative numbers of viable WT and S1PR4 KO CD8+ T cells determined by Annexin V/ 7-AAD staining at day 2 and at day 13 for this individual experiment. One representative experiment with 5 independent biological replicates is shown, which was repeated three times with similar outcomes. (G) Absolute cell number of WT and S1PR4 KO CD103+ CD8+ Trm T cells at day 13. One representative experiment with 5 independent biological replicates, which was repeated three times with similar outcomes is shown. Means ± SEM; two-tailed Student's t test; *p<0.05, **p<0.01, ***p<0.001.

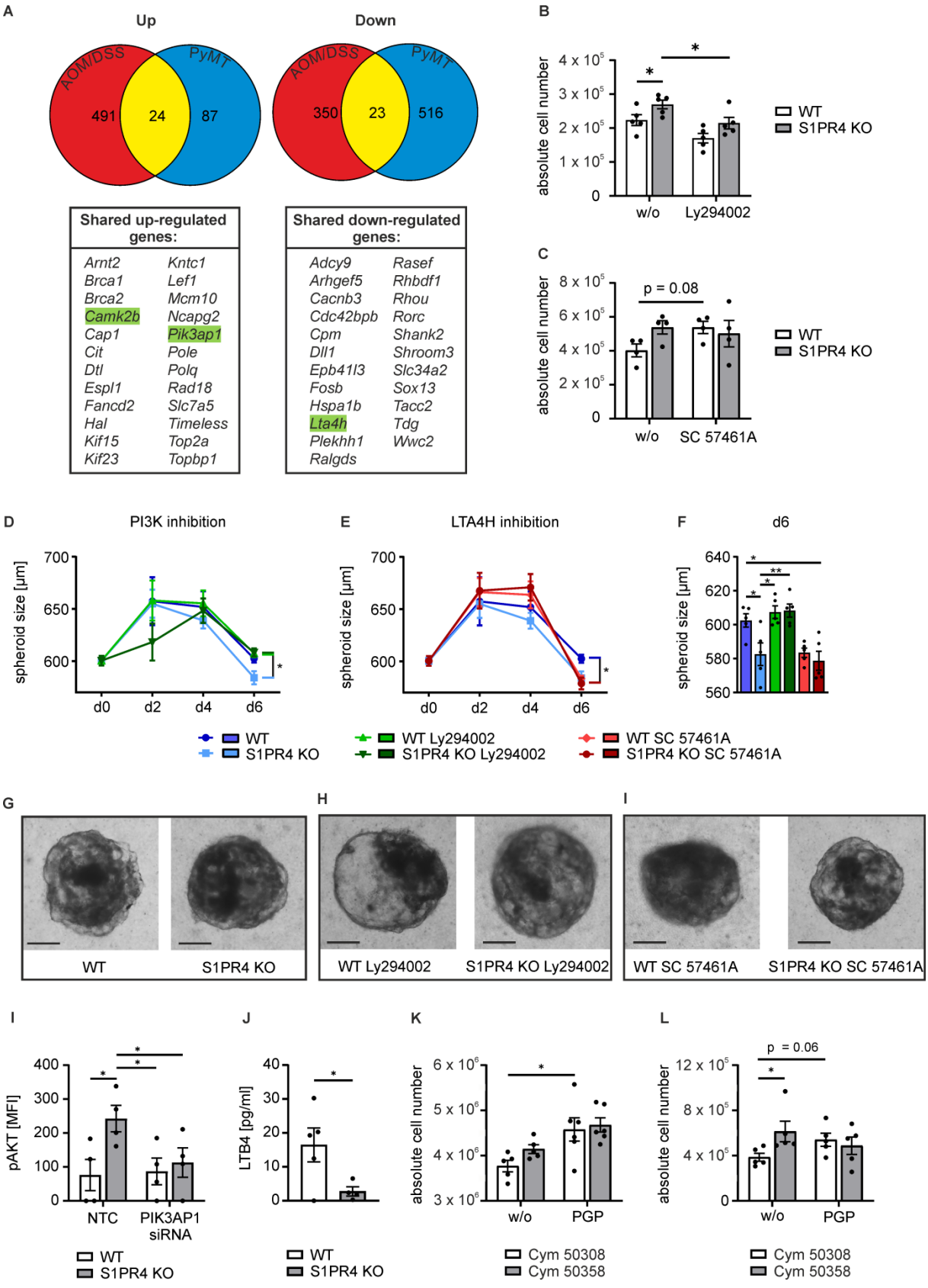

Figure 8 S1PR4 ablation promotes CD8+ T cell expansion in a cell-intrinsic manner. (A) Venn diagram and the gene list show shared and divergent up- or down-regulated genes in PyMT tumor-derived CD8+ T cells and total AOM/DSS-treated colons (day 84) comparing WT and S1PR4 KO mice. Genes selected for in vitro

validation are highlighted in green. (B, C) Absolute number of WT and S1PR4 KO CD8+ T cells either untreated (w/o) or treated with (B) 0.5 µM PI3K inhibitor (Ly294002) or (C) 5 µM LTA4H inhibitor (SC 57461A) at day 2. One representative experiment with 5 independent biological replicates is shown, which was repeated three times with similar outcomes. (D-I) PyMT tumor spheroids were co-cultured with WT and S1PR4 KO CD8+ T cells. One representative experiment with 5 independent biological replicates (each containing means of 6 technical replicates) is shown. (D-F) PyMT spheroid size upon co-culture with untreated (black), Ly294002-treated (green) or SC 57461A-treated (red) CD8+ T cells over a time course of 6 days (D, E) and at day 6 (F) after initial activation with representative photographs (G-I). Scale bars represent 200 µm. (I) Intracellular staining of phospho-AKT in non-target control (NTC) or PIK3AP1 siRNA-treated WT and S1PR4 KO CD8+ T cells 30 min post-activation (n = 4). pAKT expression is shown as mean fluorescence intensity (MFI). (J) LTB4 concentration in supernatants of WT and S1PR4 KO CD8+ T cells one day post activation determined by ELISA (n = 5). (K, L) Absolute number of S1PR4 agonist (Cym 50308) or antagonist (Cym 50358) pre-treated CD8+ T cells either untreated (w/o) or treated with 20 µM PGP 6 days (K) or 8 days (L) post-activation (n = 5). Means ± SEM; one-way ANOVA (B-F, I) or two-way ANOVA (K, L), each with Holm-Sidak's correction; *p<0.05, **p<0.01.

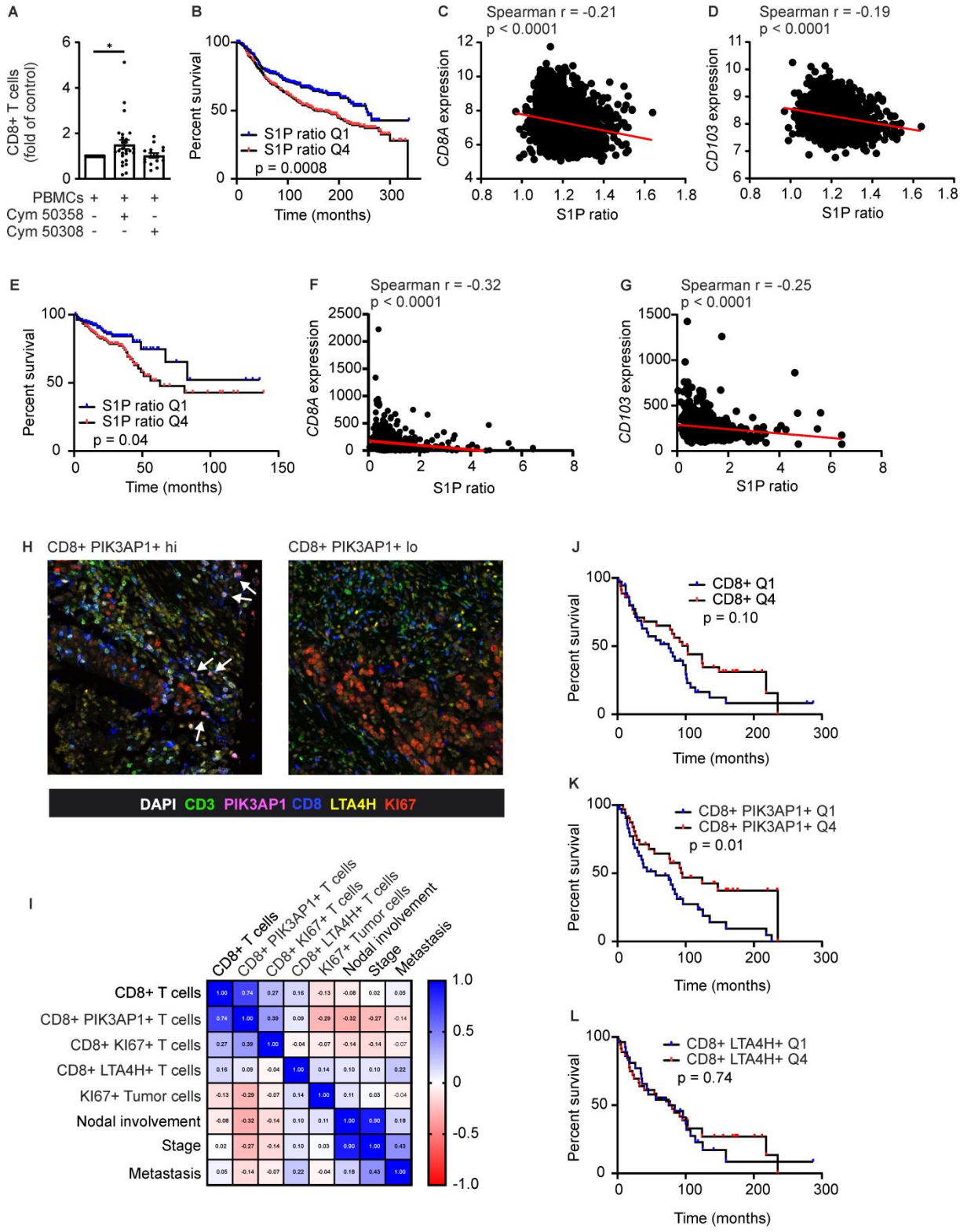

Figure 9 S1PR4-dependent alterations in CD8+ T cells are linked to human cancer progression. (A) Human PBMCs were pre-activated with 10 ng/ml of LPS and 100 U/ml IFNγ and pre-stimulated with or without 200 nM Cym50358 (S1PR4 antagonist, n = 25) or 200 nM Cym50308 (S1PR4 agonist, n = 15) for 30 min prior to being co-cultured with MCF-7 spheroids for 6 days. The relative amount of CD8+ T cells as fold of control is shown. p values were calculated using one sample Wilcoxon test. *p<0.05. (B-G) The METABRIC dataset (B-D) and the TCGA colon adenocarcinoma dataset (E-G) were used to calculate an *in silico* S1P ratio, which was

correlated with overall patient survival (B, E; Q1, 25% of patients with lowest S1P ratio; Q4, 25% of patients with highest S1P ratio) and CD8A or CD103 expression of human breast (C, D) and colon (F, G) tumors. (H-L) Tissue microarrays of human colon adenocarcinoma (H, I) and human invasive mammary carcinoma (J-L) cores were stained for CD3, CD8, PIK3AP1, LTA4H and KI67 by PhenOptics. Nuclei were counterstained with DAPI. (H) Representative images show magnified areas of colon adenocarcinoma tissue cores (full cores in Suppl. Figure 5A). Proliferating (KI67+) CD8+ PIK3AP1+ T cells are marked by arrows. Scale bars represent 50 µm. (I) Correlation matrix of CD8+ T cell subsets in colon adenocarcinoma tissue cores compared to proliferating tumor cells, nodal involvement, stage and metastasis. Spearman r-values are indicated. (J-L) Correlation of CD8+ T cell, PIK3AP1+ CD8+ T cell and LTA4H+ CD8+ T cell infiltrates in mammary carcinoma cores with overall patient survival (Q1 indicates 25% lowest abundance, Q4 indicates 25% highest abundance each).